RESEARCH

A 3D bedrock modeling method based on information mining of 2D geological map

Tong Niu[1,2] · Bingxian Lin[1,2] · Liangchen Zhou[1,2] · Guonian Lv[1,2]

Abstract

The 2D geological map serves as a synthesis of geological investigations and expert knowledge, making it a crucial data source for bedrock 3D modeling. Nevertheless, insufficient geological information mining has been a problem in previous research utilizing 2D geological maps for bedrock modeling. To address this issue, this paper proposes a 3D bedrock modeling method that incorporates multiple information mining based on 2D geological maps. The method involves extracting surface undulation, occurrence, stratigraphic age, and other information from the 2D geological map multiple times using map-cut cross sections and virtual drills. This information is then stored using the generalized trigonal prismatic (GTP) element. Additionally, the paper introduces connection rules to handle different geological phenomena, such as stratigraphic pinch-out, stratigraphic inversion, stratigraphic duplication, and unconformity contact, and their corresponding GTP types. Finally, the GTPs are connected according to these rules, resulting in the construction of a 3D bedrock model. To validate the method's consistency with expert speculation regarding the expression of geological body structures and occurrence, the paper compares a slice section of the example modeling results with expert hand-drawn section from the same location. The results demonstrate that the proposed modeling method effectively explores the geological information present in the planar geological map and clearly expresses a variety of complex geological formations, enabling the construction of a high-quality 3D bedrock model.

Keywords 2D geological map · 3D bedrock modeling · Virtual drill · Information mining · GTP

Introduction

Three-dimensional modeling of the bedrock is a crucial aspect of deep earth information exploration, as it enables the spatial representation, morphology, and topological relationships of the bedrock in three-dimensional visualization. This process holds immense significance in the interpretation and description of geological phenomena, disaster prediction, quantitative geologic simulation, and underground

resource development (Guo et al. 2021; Wycisk et al. 2009; Yang et al. 2017; Zhu et al. 2006, 2016). Currently, measured borehole and profile data, geophysical exploration data, and 2D geological maps are the three main data sources utilized to model 3D bedrock geologic entities (Hao et al. 2021).

Drills and measured profiles can effectively illustrate the spatial distribution of geological formations, structures, and stratigraphic contact relationships (Ragan 1985; Compton and Compton 1985). Modeling techniques that utilize these drills and measured sections have proven to be efficient in representing simple layered geological bodies (Abbaszadeh Shahri et al. 2020; Gong 2019; Guo et al. 2021; He and Wu 2013; Herbert et al. 1995; Marrett and Bentham 1997; Pierantoni et al. 2013; Zhang et al. 2020). However, obtaining drills and measured profiles that target bedrock can be challenging. They are often sparsely distributed, and the limited data available can impact the quality of the geological body models (Li et al. 2019; Zhang et al. 2022). Geophysical exploration data provide valuable insights into the

✉ Bingxian Lin
  linbx@njnu.edu.cn

1   Key Laboratory of Virtual Geographic Environment
    (Ministry of Education), School of Geography, Nanjing
    Normal University, Nanjing, China

2   Jiangsu Center for Collaborative Innovation in Geographical
    Information Resource Development and Application,
    Nanjing, China

🖄 Springer

geology of the deep Earth (Jørgensen et al. 2013). Several approaches effectively utilize this data for modeling purposes (Hao et al. 2016; Malehmir et al. 2008; Cai et al. 2019; Frank et al. 2007; Lysdahl et al. 2022; Høyer et al. 2015; Xin et al., 2014).

2D geological maps are generated through field geologic investigations and integrate a wealth of survey results and expert knowledge. They provide spatial and attribute information on rock formations and geologic structures from a planar perspective, including geometry, topology, age of formation, and occurrence (Schetselaar 1995). There are two primary methods for bedrock modeling using 2D geological maps: those that utilize 2D geological maps as a secondary data source and those that rely on 2D geological maps as the primary data source.

The boundaries of stratigraphic outcrops mined in these maps can be utilized as constraining rules to aid in modeling other data sources, such as measured drills, profile data, and geophysical data (Martelet et al. 2004). Martelet et al. (2004) employed geostatistical interpolation techniques to artificially construct a 3D geological model using geotectonic information from 2D geological maps. Zanchi et al. (2009) mined 3D information on faults and strata from 2D geological maps, utilizing them as constraints to construct a 3D geologic model. Wu et al. (2005) extracted stratigraphic boundary information from 2D geological maps and combined it with measured drills, real profiles, and geophysical exploration data for joint modeling. Kaufmann and Martin (2008) proposed a 3D geological modeling method based on drills, cross-sections, and 2D geological maps. Meng et al. (2009) extracted stratigraphic line information from 2D geological maps to serve as constraints, integrating multi-source data for 3D geological body modeling. Che and Jia (2019) utilized 2D geological maps and an improved fault modeling method to establish fault geometry using an enhanced Kriging interpolation approach, followed by bedrock block modeling. Hao et al. (2021) incorporated 2D geological maps as constraint data in all modeling methods to ensure consistency between the surface portion of the geologic body model and the 2D geological map. García-Gil et al. (2023) employed 2D geological maps as one of the data sources for implicit 3D modeling.

However, in certain areas, there may be a lack of or insufficient availability of other real data, which poses challenges in three-dimensional bedrock modeling (Jessell 2001; Ltd 2007). In such cases, the 2D geological map becomes a fundamental and crucial data source for modeling purposes.

Some scholars have noticed the problem and devoted themselves to researching the bedrock modeling method which takes the 2D geological map as the main data source and mines as much information as possible from the 2D geological map. Dhont et al. (2005) employed the 2D geological map to extract simple fault information and sedimentary sequencing information, constructing a 3D model of the bedrock. However, this method is only suitable for areas with relatively uncomplicated geological structures. Hou et al. (2007) characterized the 2D geological map and performed 3D fault surface modeling based on a wireframe model. The basis for 3D bedrock block modeling is laid by this method's exceptional performance in 3D fault surface modeling. Some scholars have proposed knowledge-driven modeling methods based on 2D geological maps (Xu 2014; Liu et al. 2022). However, the manually constructed geologic rule base, based on experts' experience, needs to be updated to account for the specific conditions of different regional geologies. Additionally, the constraints within the rule set for modeling complex geologic phenomena need to be expanded and improved, and the universality of this modeling approach requires further verification.

Some scholars have found that geological informations such as surface undulation, occurrence, stratigraphic age, and topological relationships in 2D geological maps can be mined into vertical upward map-cut cross sections. Zhou et al. (2013) extracted geological information from the 2D geological map and converted it into map-cut cross sections. They then rasterized these sections to construct a bedrock geologic body model using rule elements. Lin et al. (2017) utilized 2D geological maps to extract geological information. They then transformed this information into map-cut cross sections and achieved 3D modeling by geometrically constraining the relationships between stratigraphic polygons and folds on the 2D geological maps. This approach enabled large-scale bedrock modeling using 2D geological maps. However, this method only mines the information once, and its model connection method, based on wireframe relationships, can introduce errors when neighboring profiles lack correspondence. This limitation arises from the fact that the geologic information within the map-cut cross sections can be further discretized and extracted. Thus, there is room for improvement in terms of enhancing the completeness of geologic information extraction and accurately modeling the contact relationships between rock layers and the morphology of geologic formations.

However, in real geological environments, there are often additional factors to consider, such as branches, stratigraphic pinch-out, and deformation structures (e.g., faults, folds). When connecting the sections, the challenge arises in determining the corresponding geological boundaries between neighboring sections (Chen et al. 2023). This issue

can lead to a model that does not effectively represent the true geological structure.

Based on a review of prior research, it is evident that while there is significant research on 3D bedrock modeling methods based on 2D geological maps, the extraction of geologic information from these maps remains limited, and the modeling constraint rules are still imperfect. This becomes particularly challenging when there is a lack of real drills, measured profiles, and geophysical data. Therefore, there is a need for further improvement in the automated and high-complexity mining and modeling of geological information for bedrock geological bodies in a specific area using 2D geological maps as a data source. In addressing the aforementioned challenges associated with modeling using 2D geological maps, this paper aims to explore the following key issues:

- How can the extraction of geological information, such as surface relief, occurrence, stratigraphy, and stratigraphic age, be optimized from 2D geological maps? Additionally, how can the correlation between these pieces of information be maximally preserved during the multiple information extraction processes?
- How can appropriate information aggregation rules be devised to model different complex geological formations, including stratigraphic pinch-out, stratigraphic inversions, stratigraphic duplications, and unconformities, using the extracted information?

To address the aforementioned key issues, this paper presents a novel approach for 3D bedrock modeling that involves multiple mining of geologic information from 2D geological maps. The proposed method offers the following contributions:

- Building upon previous research on the initial information extraction from 2D geological maps using map-cut cross sections, this paper introduces a second information extraction method based on virtual drills. This method aims to discretize and condense the information obtained from the map-cut cross sections into virtual drills.
- The data structure in both information mining scenarios is designed to preserve the correlation between 2D geological maps, map-cut cross sections and virtual drills so that, despite their apparent discreteness, they are actually tightly correlated;
- Using the generalized trigonal prism (GTP) spatial data model (Wu 2004), this study examines the composition of the GTP by considering three virtual drills as its vertices. The paper discusses the specific combinations of virtual drills within the GTP for various geological

phenomena, including normal sedimentary strata, stratigraphic pinch-out, stratigraphic inversions, stratigraphic unconformities, and more. Furthermore, the corresponding GTP connection rules are established to account for different scenarios;

- Based on the defined connection rules, the discrete geological information stored in the virtual drills is aggregated to establish a three-dimensional model of the bedrock geological body that aligns with the inferences drawn by geologists.

In the subsequent sections, this paper is organized as follows: The fundamental concept of the proposed modeling approach is presented in Sect. Basic idea, while Sect. Methodology offers a detailed explanation of the current modeling methodology. To validate the effectiveness of the proposed approach, modeling experiments and validation analyses are conducted in Sect. Experimentation and analysis. Section Discussion critically examines the accuracy and limitations of the present method, highlighting its advantages over previous modeling approaches. Finally, Sect. Conclusion concludes the paper, summarizing the results and suggesting potential avenues for future research.

Basic idea

The paper proposes a method for extracting geological information from 2D maps through two information mining processes. The first stage involves extracting parameters like elevation change, occurrence, topological relationships, stratification, and age. This data is organized into map-cut sections. The second stage further extracts information from these sections, which is then discretized into virtual drills. It is crucial to establish a mapping method that preserves correlation relationships between the map, cross sections, and drills. The extracted information and association relations are integrated into the virtual drills using the GTP element model to construct a 3D geological model during stage 3. Figure 1 illustrates all the stages.

Methodology

This paper's modeling approach can be divided into three main parts. Firstly, information mining is done using map-cut sections. Secondly, virtual drills are used for information mining. Lastly, an integrated 3D bedrock modeling is achieved by applying GTP connection rules to consolidate the extracted information.
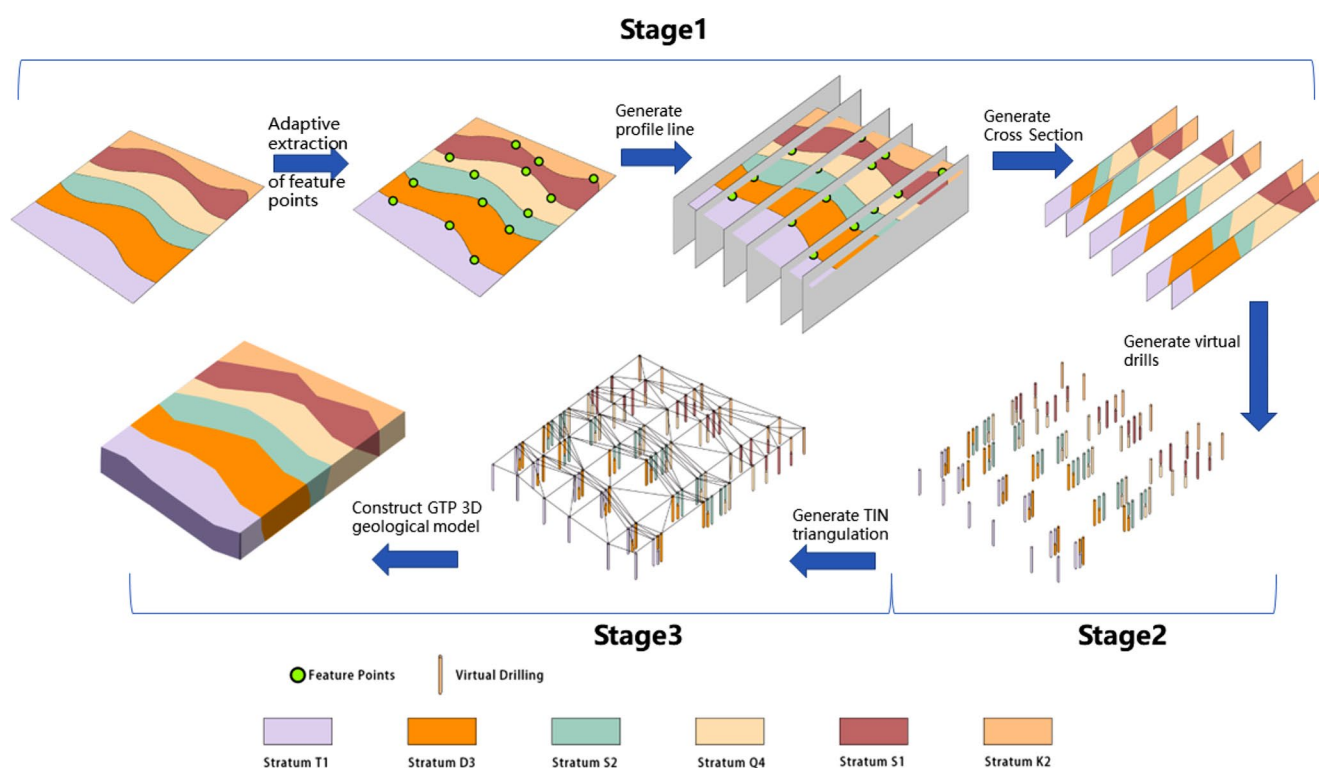
Fig. 1 Three stages of the proposed 3D modeling of geologic body based on 2D geological map knowledge mining

Input data for bedrock modeling based on information mining

The data utilized for information mining in this paper consists of the following components:

- 2D geological map: This includes stratigraphic lines, fault lines, and stratigraphic planes. These elements provide essential information for modeling bedrock geologic bodies, such as stratification, formation age, boundary lines, fault lines, and spatial locations.
- Elevation data: This includes DEMs and contour lines, providing elevation information like surface relief.
- Occurrence data: An important rock formation, refers to the spatial location of various tectonic surfaces. The occurrence elements, such as strike, inclination, and dip, determine the placement of these tectonic surfaces. Occurrence point data provides relevant information for these features.

Please refer to Fig. 2 for a visual representation of these data components.

First information mining of 2d geological maps based on map-cut cross sections

This stage involves extracting geological information and correlations from a 2D geological map, including surface relief, stratigraphic stratification, formation age, and production status. This creates map-cut sections that map elements between the 2D map and cross sections. The stratigraphic lines and polygons in the cross sections correspond to rock strata on the map. Elevation information from contour data and DEM accurately represents ground undulations, transforming it from 2D to 3D. Figure 3 shows the flow of the method mentioned herein for automated drawing of map-cut profiles. Also, Fig. 3 shows the correspondence between information in map-cut sections and the 2D geological map. zhoulao

Adaptive generation of profile lines based on the characterization of outcrop lines on 2d geological maps

The initial step in batch generating map-cut sections involves constructing adaptive profile lines using stratigraphic line characteristics. Accurate modeling relies on properly spaced and parallel profile lines. To determine spacing, consider variations in slope along outcrop lines. Gradual slope changes require sparser arrangement, while areas with greater curvature and slope variability require
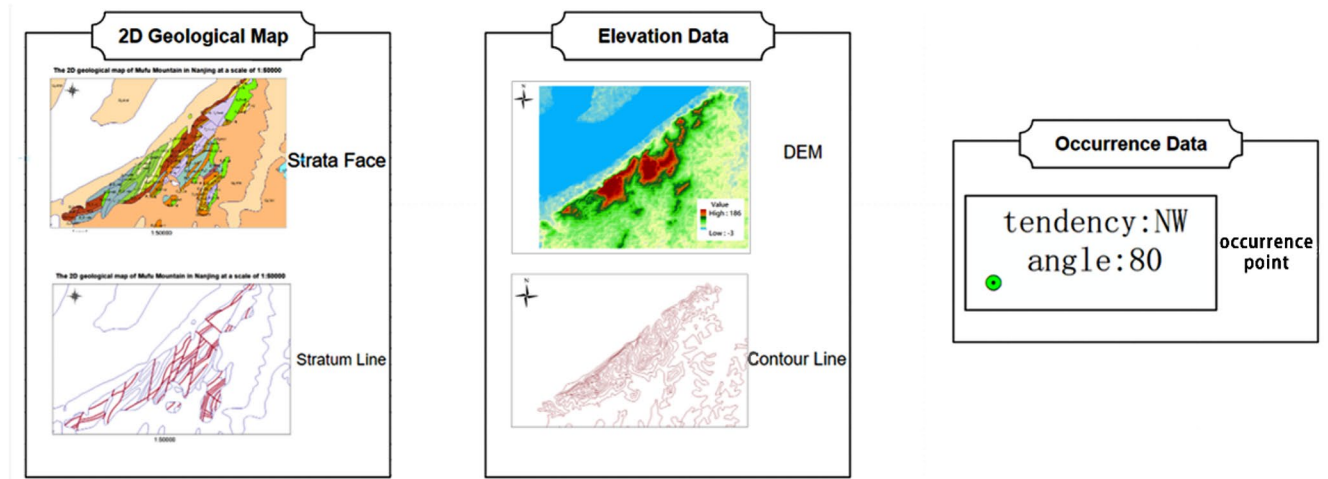
Fig. 2 The 2D Geological Map Dataset used in this article
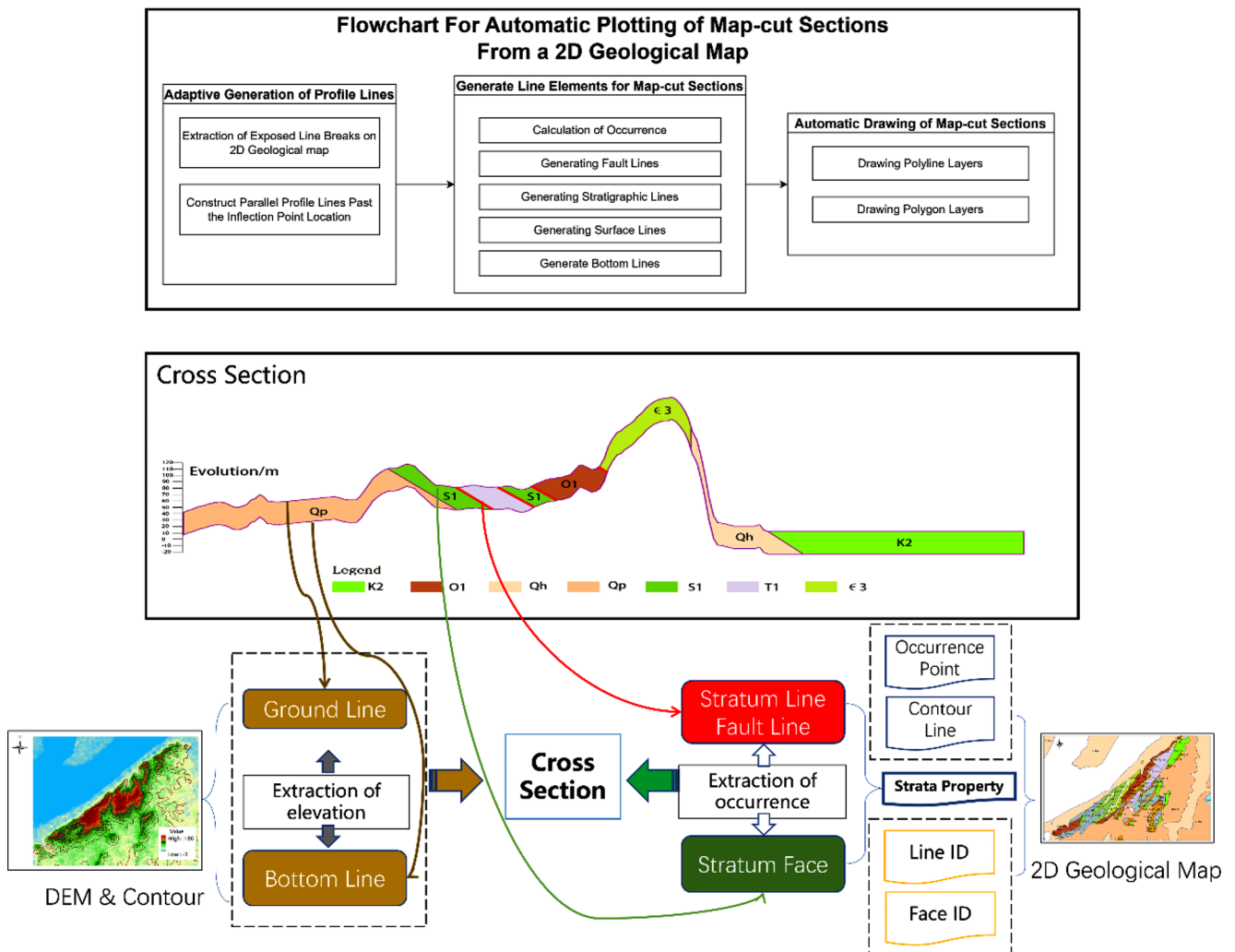

Fig. 3 Process of automatic generation of map-cut sections and correspondence of geologic information in 2D geological maps and map-cut sections
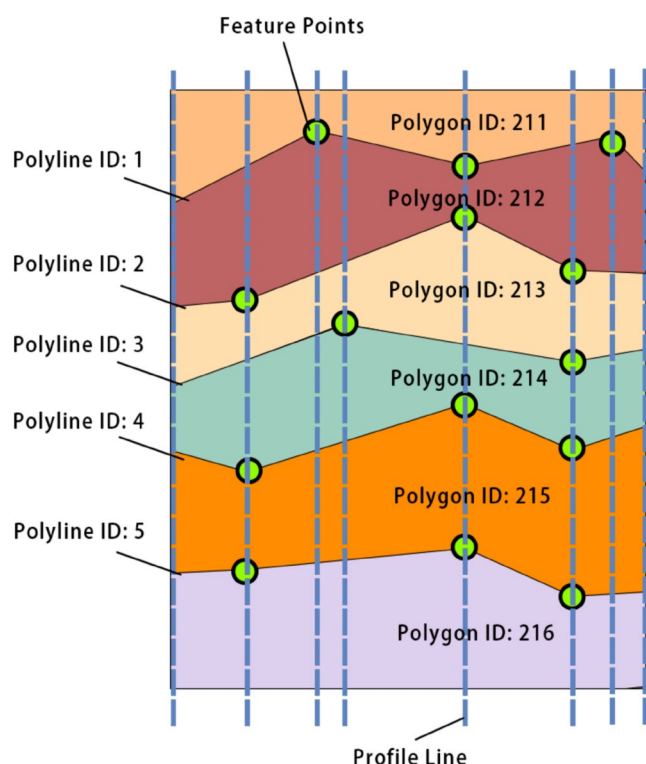
Fig. 4 Adaptive Construction of Profile Lines

represents geological features. Please refer to Fig. 4 for a visual representation of the adaptive construction of profile cutting lines.

Methods for generating map-cut cross sections based on profile lines

The occurrence information extracted from the 2D geological map and the surface relief data obtained from the DEM are represented in the line elements of the map-cut cross sections. Additionally, details related to the topological relationships between ground surfaces, the stratification of rock layers, and the age of rock formation are extracted and associated with the surface elements of the map-cut sections. To construct the map-cut cross section, this paper adopts the method described in Lin et al. (2017).

Figure 5 illustrates the process of extracting the initial information from a profile line location on the 2D geological map. Here, DSN and DSO represent the formation age name and code, respectively.

Firstly, we intersect the original profile line with the 2D geological map line elements and retrieve elevation information for the intersection point from the DEM. Next, we calculate the occurrence element of the point. There are two methods for determining the occurrence element of a point: the direct method and the indirect method.

(1) Direct method: The stratigraphic occurrence elements at the target location are derived through inverse distance weight interpolation, using the available discrete occurrence point data. However, if the number of occurrence

closer positioning. This adaptive approach preserves the curvature characteristics of stratigraphic outcrop lines. Rock layer surface characteristics correspond closely to the turning points of outcrop lines on the 2D geological map, such as stratigraphic and fault lines. By extracting these points and constructing parallel profile lines, this method precisely
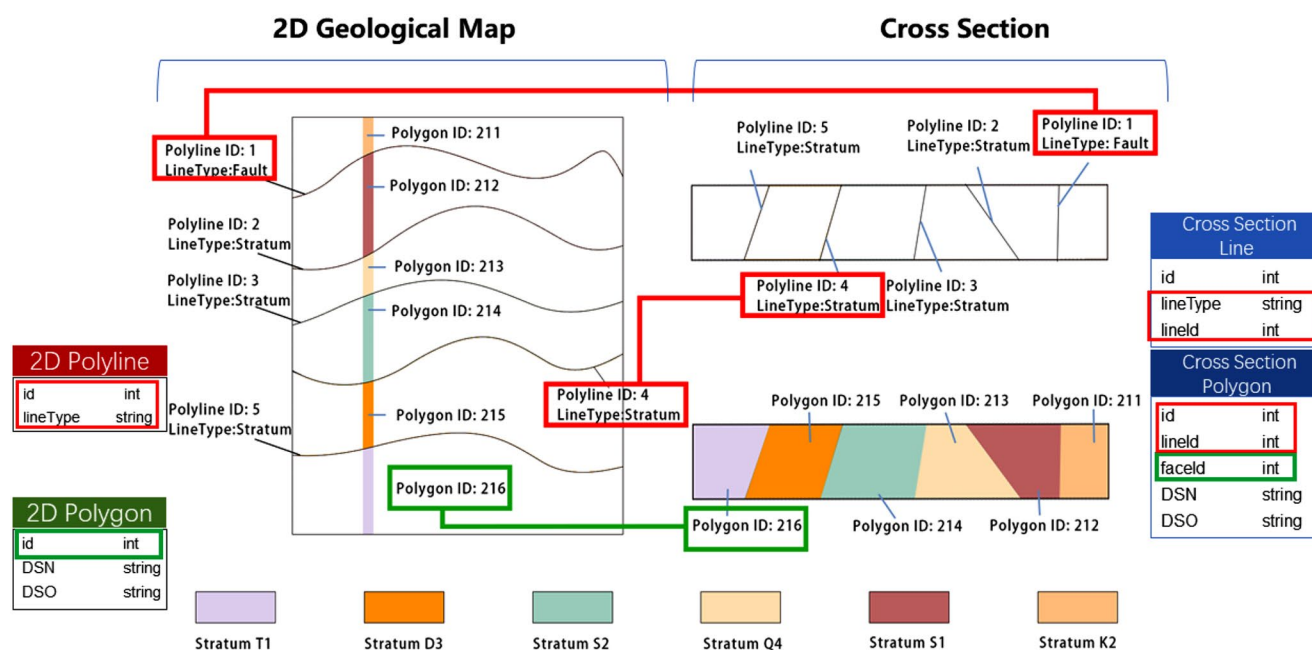

Fig. 5 Mining geological information and relational information in 2D geological map to the cross sections

points is limited or non-existent, the calculated results will exhibit significant bias.

(2) Indirect method: When the direct method is not applicable, the indirect method is used to calculate occurrence elements (Zhou et al. 2013). By combining the definition of occurrence with stratigraphic line and contour data, the occurrence element of the target stratigraphic level is determined.

Figure 6 demonstrates an inclined stratum intersecting with two contour lines at strike lines I and II, respectively (Fig. 6a). If two parallel strike lines of different heights, adjacent to each other, are obtained within the same stratum, the occurrence information of the stratum can be derived using its elevation and horizontal distance. Refer to Fig. 6b for the plan view.

Equation (1) was subsequently applied to determine the true dip angle and slope of the stratigraphic lines in the profile. This information was then utilized to draw the stratigraphic lines, as Fig. 5 depicted.

$$\beta = \tan^{-1}\left[\tan\alpha * \cos(\gamma - \delta)\right] \qquad (1)$$

where β represents the true angle of dip, γ signifies the profile line strike, δ denotes the dip, and α represents the sight dip. This method utilizes surface undulation information to establish surface and bottom lines, and occurrence information to determine stratigraphic and fault lines. These elements collectively form the line components of the map-cut section (Fig. 5).

Stratigraphic information is embedded in the attribute values of the 2D geological map surface elements (Polygon in Fig. 5). When the location of a profile line is determined on a 2D geological map, it is interrupted by seeking intersection with stratigraphic lines, fault lines, etc. Thus, the profile line is divided into several consecutive line segments on the 2D plane (Fig. 5). By determining the coordinates of the midpoint for each line segment on the 2D plane of the 2D geological map, we can extract stratigraphic

age information associated with those points. Utilizing the stratigraphic age data from these 2D points, we can assign corresponding attribute values to all profile line segments and stratigraphic polygons within the map-cut cross section.

To preserve the mapping relationship between the 2D geological map elements and the map-cut section, key values are assigned to stratigraphic lines and fault lines (PolylineID and LineType in Fig. 5). These values are associated with their counterparts in the section. Similarly, unique key values are assigned to stratigraphic faces in the 2D geological map, serving as association information for profile face elements (PolygonID in Fig. 5). These key-values structure enables the association between map elements and profile information.

To facilitate readability, we present the pseudo-code for generating graph-cut profile line elements (as depicted in Fig. 7). Similarly, line elements in the map-cut section of can be converted to face elements. Subsequently, following the approach outlined earlier, we can extract the relevant stratigraphic attribute information from the 2D geological map and assign it to the corresponding face element.

Second information mining of map-cut cross section based on virtual drills

Virtual drill data structure

To model intricate geological formations, map-cut sections require additional mining and discretization. We design the Virtual Drill data structure for this purpose, storing outcomes of the second information mining process (Fig. 8a). The Virtual Drill stores planar coordinate information, along with a column of virtual strata sharing the same coordinates. Each Virtual Stratum contains geological information and correlations from the map-cut section, along with absolute elevations (zUp, zDown) of its top and bottom boundaries. To establish associations with the virtual strata, each virtual drill is assigned a unique mapping key value (id).

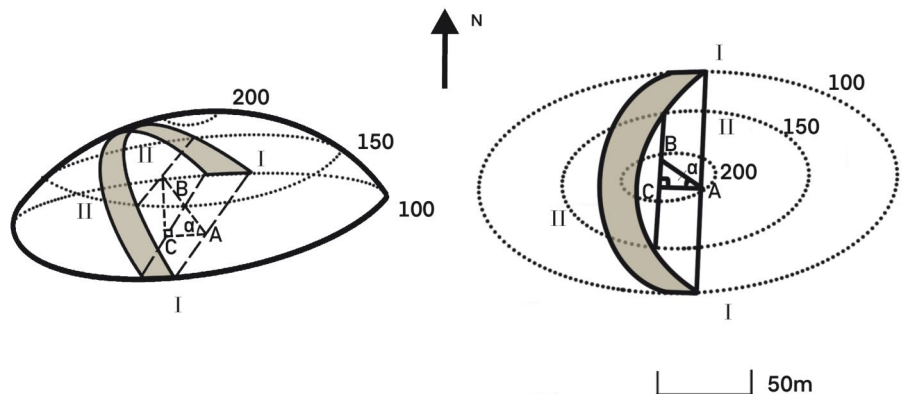**Fig. 6** Indirect method of occurrence information (based on Zhou et al. 2013)

Fig. 7 Pseudo-code for drawing stratigraphic lines in the first information mining

---

Algorithm 1 *Automatic generation of line elements for map − cut sections*

1: **procedure** LGEN$(2DMap, profileLine, DEM, occurrences, contour)$
2:     $lineList \leftarrow empty$
3:     **Obtain all intersections of the profile line with the stratigraphic line**
4:     $pointCollectionAll \leftarrow$ new empty List
5:     **for** $i \leftarrow 0$ **to** $2DMap.Polyline.Count$ **do**
6:         $targetPolyline \leftarrow 2DMap.Polyline[i]$
7:         **if not** $profileLine$ and $targetPolyline$ Intersect **then**
8:             **continue**
9:         **end if**
10:         $pGeometry \leftarrow profileLine.Intersection(targetPolyline)$
11:         $pointCollection \leftarrow pGeometry.Coordinates$
12:         $pointCollectionAll.Add(pointCollection)$
13:     **end for**
14:     **Obtain all intersections of the profile line with the fault line. The code is omitted here to keep things simple**
15:     **for** $i \leftarrow 0$ **to** $pointCollectionAll.Count$ **do**
16:         $ssPoint \leftarrow pointCollectionAll[j]$
17:         $ssPoint.Z \leftarrow DEM.GetRasterValue(ssPoint.X, ssPoint.Y)$
18:         **Get the specific stratum line/fault line where the ssPoint is located on the 2D geological map.**
19:         $tempStratum \leftarrow GetPolylineByPoint(ssPoint, 2DMap)$
20:         **Calculate the occurrence of intersection by direct or indirect method**
21:         $angleDip, dip \leftarrow GetOccurence(tempStratum, countour)$
22:         $strike \leftarrow GetLinestrike(ssPoint, occurrences)$
23:         $sightDip \leftarrow \arctan\left(\tan(angleDip \times \frac{\pi}{180}) \times \cos(strike - dip \times \frac{\pi}{180})\right)$
24:         **Setting the vertical thickness of the profile and calculating the upper and lower boundary points**
25:         $upperPoint \leftarrow$ GetLocation$(ssPoint, profileLine)$
26:         $lowerPoint.X \leftarrow upperPoint.X + \frac{straThickness}{\tan(sightDip)}$
27:         $lowerPoint.Y \leftarrow upperPoint.Y - straThickness$
28:         $crossPolyline \leftarrow$ ConvertPoints2Line$(upperPoint, lowerPoint)$
29:         $lineList.Add(crossPolyline)$
30:     **end for**
31:     **Draw surface and bottom lines on the cross section based on the DEM and profile line. For the sake of keeping the code concise, it will not be repeated here**
32:     $lineList.Add(surfaceLine)$
33:     $lineList.Add(bottomLine)$
34:     $crossSectionShp \leftarrow$ ConvertLineList2Shp$(lineList)$
35:     **return** $crossSectionShp$
36: **end procedure**

Adaptive construction method for virtual drills based on map-cut cross section features

The selection of points for virtual drills, similar to map-cut profile lines, depends on the characteristics of the map-cut section. Figure 8b shows the steps for constructing virtual drills from a single profile.

(1) Extract feature points from the map-cut cross sections, including folds, stratigraphic lines, and fault lines. Calculate the positions of virtual drills in the plane. Ensure that virtual
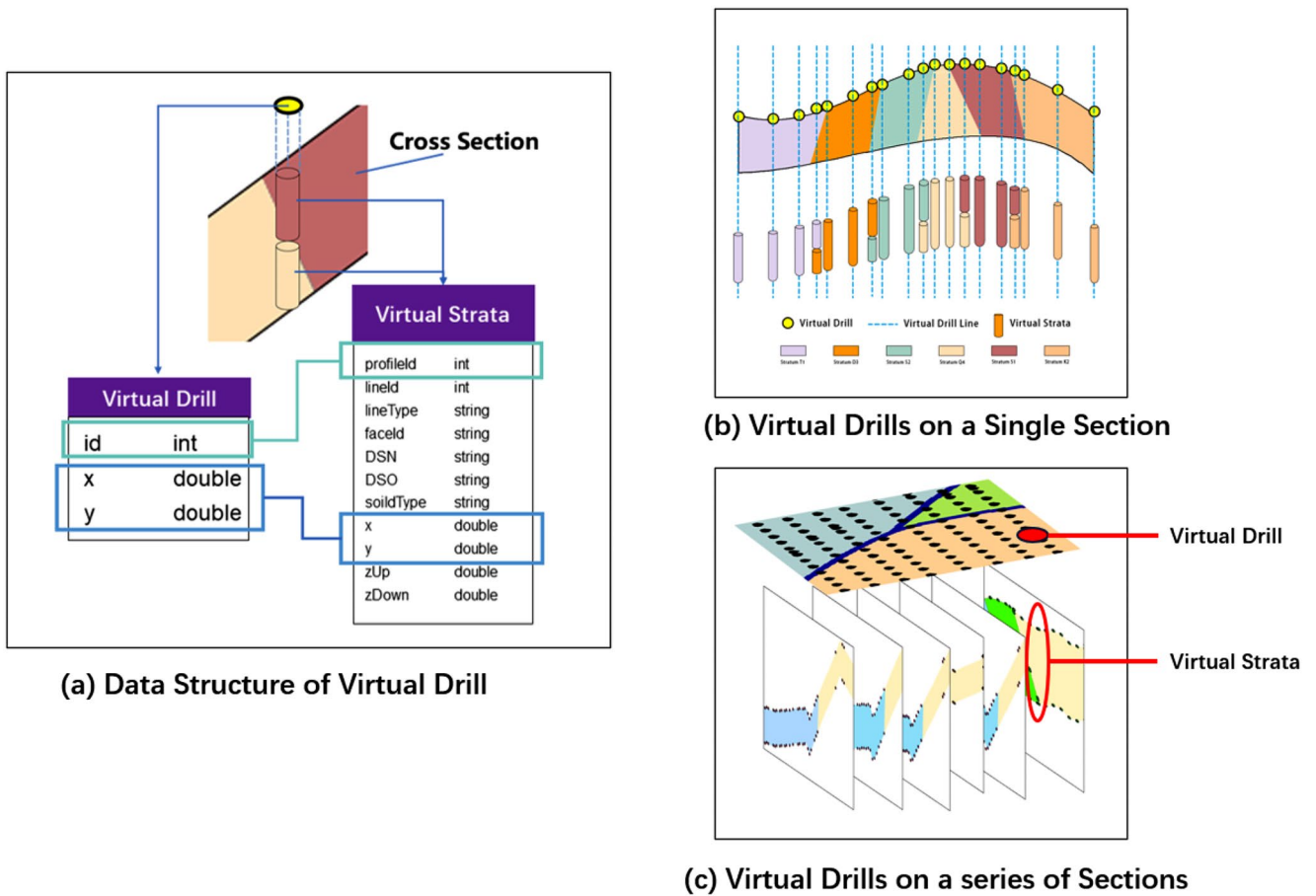
Fig. 8 Adaptively Construct Virtual Drill and Virtual Strata from Single section. (**a**) Data Structure of Virtual Drill. (**b**) Virtual Drills on a Single Section. (**c**) Virtual Drills on a series of Sections

drills are generated for each stratigraphic line/fault line on the map-cut section at the location of the starting point and intersection with the bottom line. Ensure at least one virtual drill is generated in the middle of each stratigraphic line or fault line on the map-cut cross section.

(2) Create vertical virtual drill lines at each virtual drill point. Determine the intersection point with the cross sections to establish the stratigraphic position of the virtual stratum along the virtual drill line (zUp, zDown).

(3) Mine stratigraphic layering information, such as formation age, production, and correlation information of stratigraphic demarcation points, from the map-cut section to the virtual strata.

Figure 8c illustrates the outcome of the second phase of information mining. This phase aims to create virtual drill locations in the horizontal plane and construct corresponding virtual stratigraphy vertically. The goal is to transform and consolidate geological information from the map sections into virtual drills while maintaining correlation with the map-cut sections. Despite the discrete

representation on the surface, there is a tightly interconnected relationship between them in reality.

3D bedrock modeling based on GTP

After two rounds of information mining, the geological data and correlation from the 2D map are stored in the 3D drill set. The next step involves 3D modeling and visualization using this stored information. The paper uses the multilayer generalized trigonal prismatic (GTP) metamodel as the spatial data model, chosen for its flexibility in representing stratigraphic contact surfaces and inter-strata relationships (Wu 2004). The process starts by constructing an irregular triangular network (TIN) using virtual drill locations as vertices. Virtual drills and strata within each triangular surface are interconnected, forming multi-layer GTP voxels. Finally, these GTP voxels combine to create a comprehensive 3D geological model.

Surface irregular triangular network generation based on drill locations

This paper constructs a Delaunay triangular network using the point locations and top point elevations of virtual drill points from the previous step as the data source for TIN construction. Figure 9a displays the planar point locations of discrete drill points, while Fig. 9b shows the TIN constructed using the planar point elevation information. The three virtual drills on the plane form an irregular triangular surface, with each surface representing the projection of the GTP model. Figure 9c illustrates the relationship between the GTP trigonometric model structure and the surface triangular surface.

Construction and modeling of connection rules based on gtp combinatorial classification

After the second round of information mining, geological information and correlation data are stored in virtual stratigraphic columns associated with each virtual drill point. However, this paper specifically focuses on GTP voxels, which consist of three virtual drills. A challenge arises when the stored information differs among these three virtual drills. Therefore, it becomes necessary to explore modeling methods that accommodate various scenarios of GTP compositions. In this subsection, virtual drill combinations forming GTP voxels are categorized, and corresponding GTP connection rules are discussed based on this categorization. Additionally, modeling results for the corresponding GTP voxels are presented.

Classification of GTP drill combinations In this sub-section, the stratigraphic homogeneity of the three virtual drills

that constitute the GTP will be classified based on the characteristics of the layered bedrock geologic bodies, such as continuity and sequentiality. This classification is essential for establishing the rules governing the connection of the GTP body elements.

(1) Descriptive classification of GTP drill combinations

When characterizing geologic bodies in stratified bedrock, two dimensions are considered: vertical continuity and the sequential nature of stratigraphic sequences.

- Vertical continuity is classified as continuous (**c**) or discontinuous (**d**) based on chronological breaks in formation, including stratigraphic unconformities and duplications.
- The sequence of stratigraphic sequences refers to the chronological arrangement of rock formations and can be sequential (S) or inverted (I). Typically, deposition follows oldest to newest, but tectonic movements can lead to inversion.

The process of classifying sedimentary rock features based on these dimensions is called descriptive classification. We focus on phenomena like continuous and inverted strata, parallel and angular unconformities, and stratigraphic pinch-out. We utilize the mentioned dimensions to classify these phenomena (Fig. 10). The stratigraphic pinch-out phenomenon (e.g., Fig. 10f) can exhibit both sequential and inverted characteristics, lying between continuity and discontinuity.

Virtual drills are also classified based on these dimensions (Fig. 9). Note that the stratigraphic pinch-out phenomenon
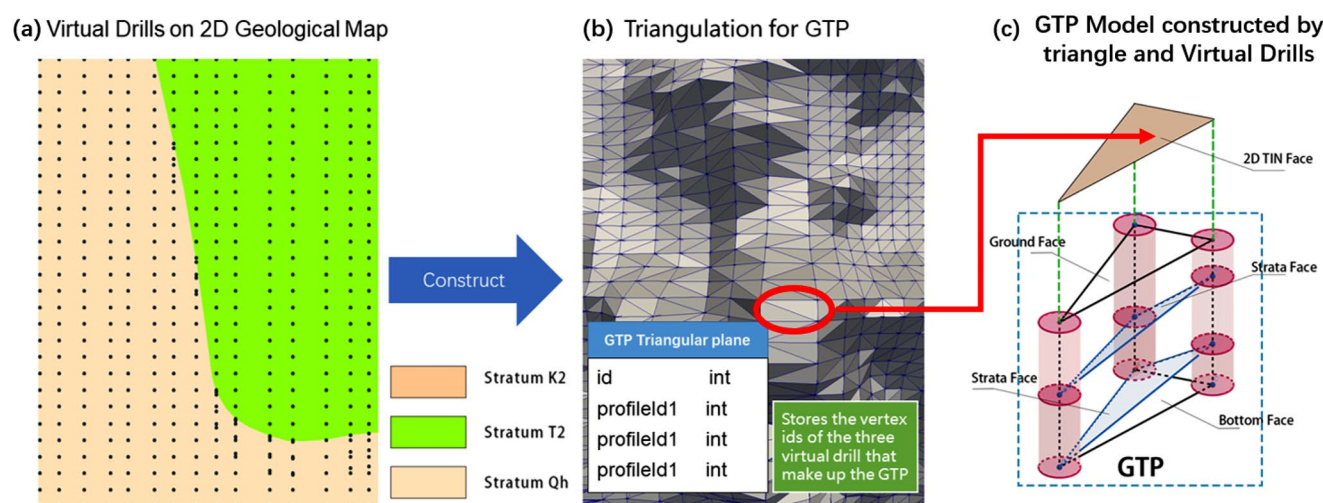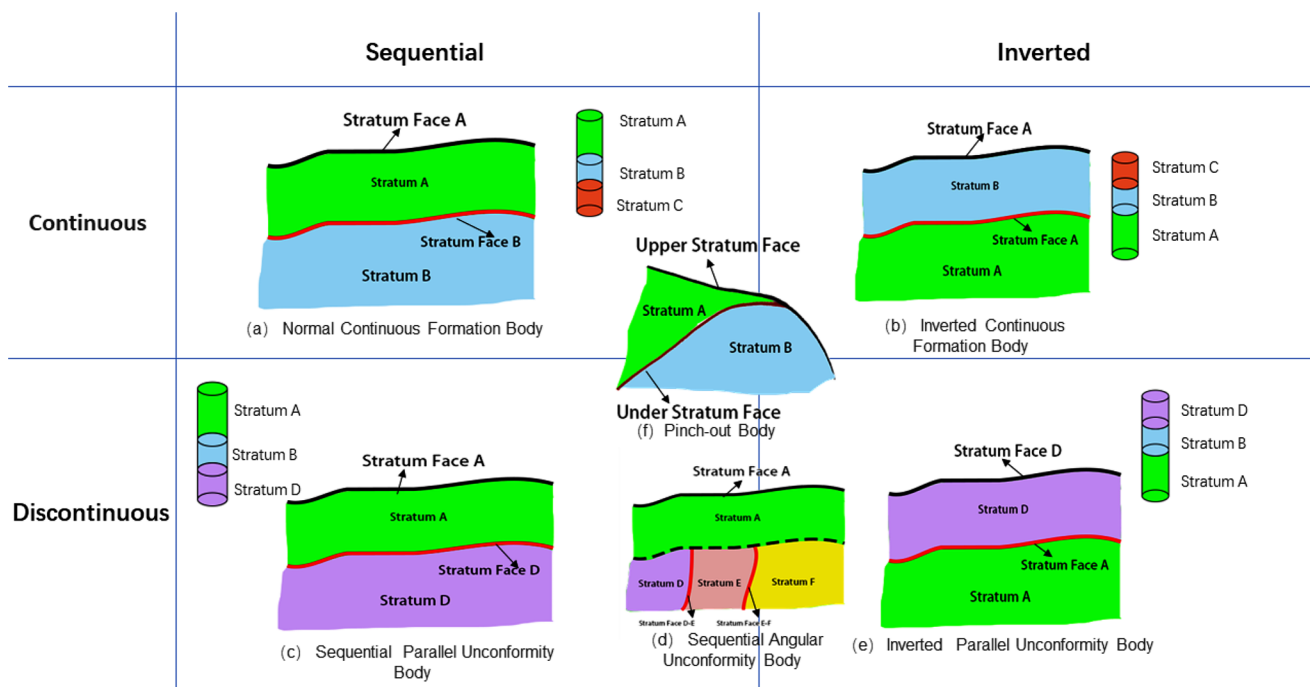

Fig. 9 Construct TIN and GTP models with virtual drills. (**a**) Virtual Drills on 2D Geological Map. (**b**) Triangulation for GTP. (**c**) GTP Model constructed by triangle and Virtual Drills

P.S. The age of the strata has aged from A to F.

Fig. 10 Distribution of drilling strata and Special tectonics from two aspects: continuity and sequentiality. (**a**) Normal Continuous Formation Body. (**b**) Inverted Continuous Formattion Body. (**c**) Sequential Parallel Unconformity Body. (**d**) Sequential Angular Unconformity Body. (**e**) lnvered Parallel Unconformity Body. (**f**) Pinch-out Body

cannot be observed in a single drill, so it is not included in the classification.

Geological formations are modeled using GTP voxels formed by combining three virtual drills. Before discussing complete connection rules, the possible GTP voxel combinations need to be classified based on descriptors.

Each drill has four descriptive cases, resulting in a total of 20 GTP cases formed by three drills (e.g., Fig. 11). The calculation formula is as follows:

$$C^3_{4+3-1} = 20 \tag{2}$$

For the sake of clarity, we have coded the combinations of the three drills that form the GTP based on "quantity," "sequentiality," and "continuity." We use "CS" for sequentially continuous virtual drills and "DI" for discontinuous and inverted virtual drill holes. We use "DS" to represent sequentially discontinuous virtual drills, and "CI" to represent continuously inverted virtual drills. For example, "3CS" means that the GTP consists of three virtual drills that are all sequential, while "2CS + 1DI" means that of the three virtual drills that make up the GTP, two are sequentially continuous and one is discontinuous and inverted.

Considering real geological constraints, the three virtual drills in the GTP won't exhibit abrupt variations in sedimentary properties. They won't feature both inverted

(I) and sequential (S) combinations (Fig. 11i and t). Consequently, the descriptive combinations can be reduced to eight cases (Fig. 11a and h). Single stratigraphic drills can be described as CS or CI.

(2) Identity classification of GTP drill assemblies

The enumeration reveals that drill combinations within the same descriptor can differ based on the age of the specific strata. In Fig. 12a, the three 3CS combinations have different connectivity outcomes. While Fig. 12a1 can be connected based on stratigraphic correspondence, Figures 12a2 and 12a3 and 12a3, with different formation dates, cannot be connected. Therefore, descriptive classification alone is insufficient to discuss GTP connectivity rules; the formation age composition also needs consideration.

The three virtual drills have three columns of sub-stratigraphy, representing combinations based on formation age. Depending on their degree of identity:

(1) Identical: the three assemblages are identical;

(2) Partially identical: there are sub-stratigraphic formations of the same age in two of the three combinations, but the three combinations are not identical;

(3) Completely different: each sub-stratum of the three drills has a completely different age.

Fig. 11 Classification results of GTP composed of 20 kinds of virtual drills according to descriptive classification. (**a**) 3CS. (**b**) 3DS. (**c**) 3DI. (**d**) 3CI. (**e**) 2CS+1DS. (**f**) 1CS+2DS. (**g**) 2DI+1CI. (**h**) 1DI+2CI. (**i**)1DI+2DS. (**j**) 2DI+1DS. (**k**)1CS+2CI. (**l**)2CS+1CI. (**m**) 1DI+2CS. (**n**) 2DI+1CS. (**o**) 1CI+2DS. (**p**) 2CI+1DS. (**q**) CS+DI+CI. (**r**) CS+CI+DS. (**s**) CS+DS+DI. (**t**) DS+DI+CI
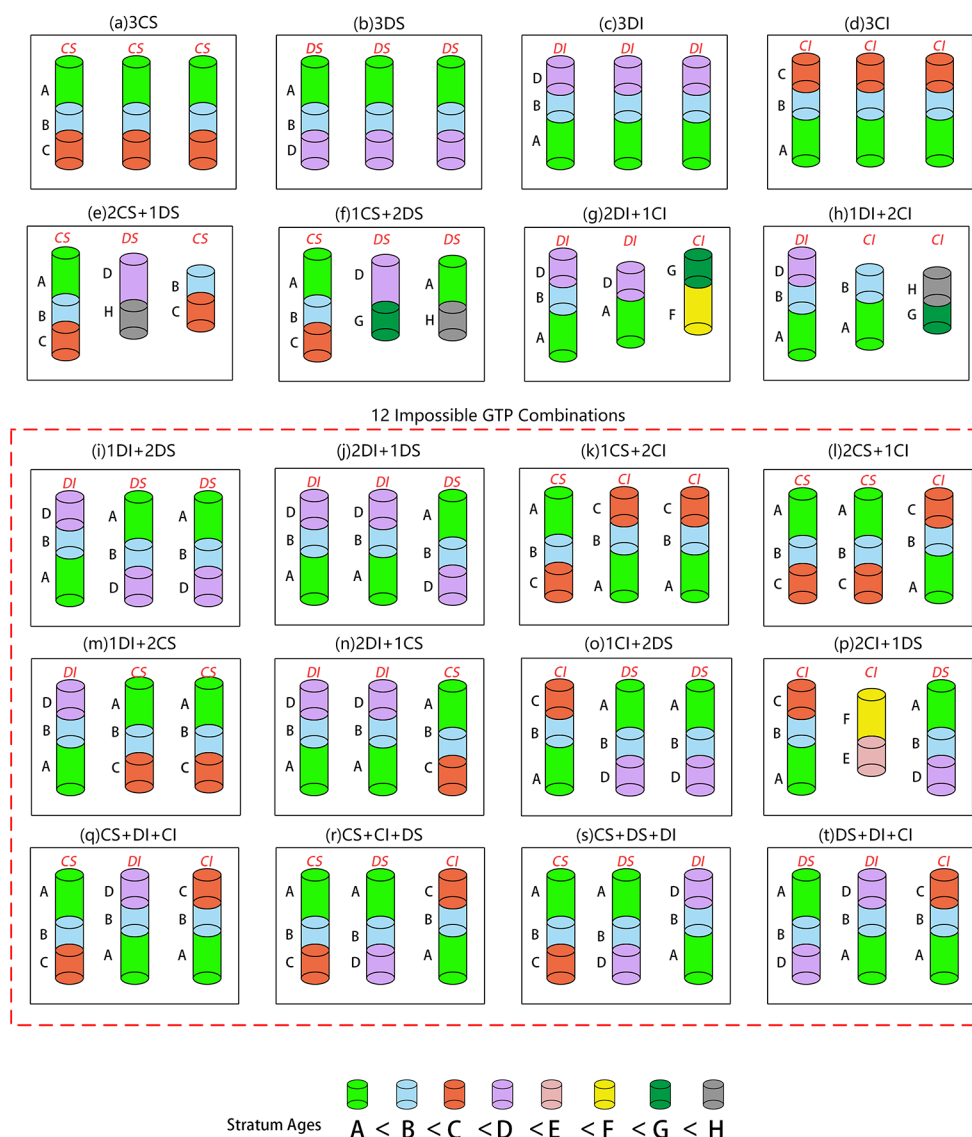
Among the various descriptive classifications, only four classifications (3CS, 3DS, 3DI, 3CI) exhibit identical compositions across all three drills (Fig. 12a1, 12b1, 12c1, 12d1), totaling four cases. Additionally, there are four classifications that have partially identical and completely different compositions, resulting in a total of eight cases. The remaining four descriptive classification results (2CS + 1DS, 1CS + 2DS, 2DI + 1CI, 1DI + 2CI) involve stratigraphic age components that are either the same or completely different, resulting in eight more cases. Therefore, after considering both the descriptive and sameness classifications, there are a total of 20 possible combinations in terms of drill compositions.

GTP connection rule construction and modeling In subsection Classification of GTP drill combinations, the classification of GTP voxels comprising the drills was performed. This subsection then summarizes three GTP linkage rules: correlation-based linkage, stratigraphic chronological order-based linkage, and a combination of correlation-based and stratigraphic chronological order-based linkage.

(1) Correlation-based linkage

Correlation-based linkage means using only correlation information mined from the 2D geological map as a linking rule between virtual drills. When the three virtual drills constituting the GTP element are these cases (3CS,

Fig. 12 The 8 descriptive classification results were further classified using similarity classification. Horizontal axis title: (1) Identical. (2) Partially Identical. (3) Completely different. Vertical axis title: (**a**) 3CS. (**b**) 3DS. (**c**) 3DI. (**d**) 3CI. (**e**) 2CS+1DS. (**f**) 1CS+2DS. (**g**) 2DI+1CI. (**h**) 1DI+2CI
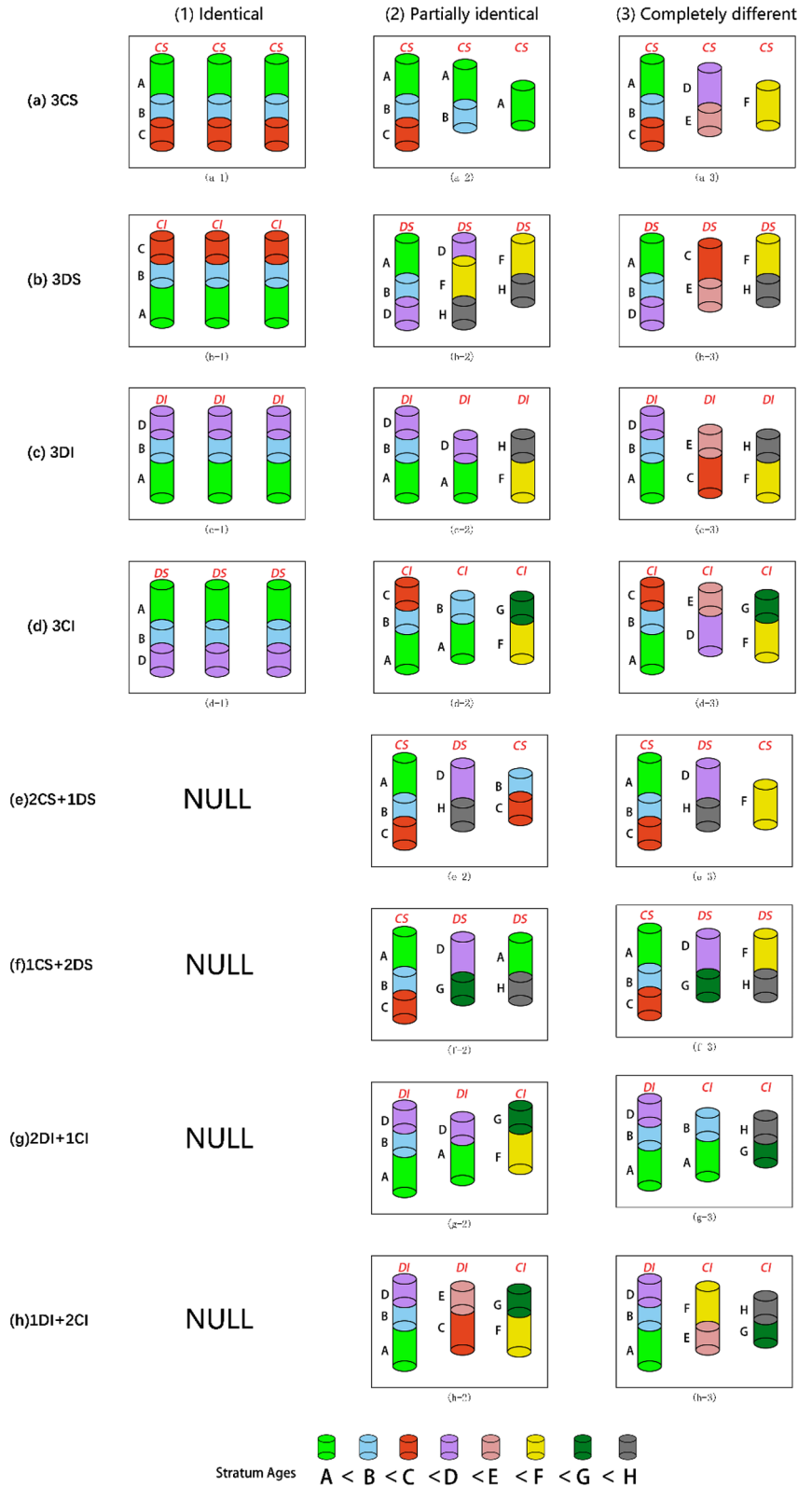
3CI,3DI,3DS) and the stratigraphic homogeneity is identical (Fig. 12a1, Fig. 12b1, Fig. 12c1, Fig. 12d1), i.e.:

$$\text{Drill } 1 = \text{Drill } 2 = \text{Drill } 3 \tag{3}$$

This is the most common scenario where the three drills share the same stratigraphic descriptive classification and exhibit the same distribution of layers and strata.

Figure 13 illustrates the correspondence between the four GTP classifications and the actual geological scenario. Specifically, Fig. 13a represents sequential continuous strata, Fig. 13b represents sequential inverted strata, Fig. 13c represents inversion-parallel unconformity strata, and Fig. 13d represents sequential parallel unconformity strata.

When the aforementioned four cases occur, the three virtual drills not only share the same geological formation date but also possess identical correlation information. This means that they belong to the same stratigraphic level on the planar geological map. In such instances, the connection rule is to link the three virtual drills based on the discovered association information and the mapping relationship between virtual strata, as depicted in Fig. 14.

(2) Stratigraphic chronological order-based linkage

Stratigraphic chronological order-based linkage is a rule that uses only chronological information about strata excavated from 2D geological maps to link virtual drills to each other based on stratigraphic chronological order. The chronological order of bedrock formation is a natural stratigraphic connectivity rule. Due to the strong chronological relationship of stratigraphic distributions, in general, strata of earlier ages generally underlie strata of later ages. When the form of stratigraphic assemblage of the three drills that make up the GTP is completely different, i.e.:

$$\text{Drill1} \cap \text{Drill3} = \varnothing, \ \text{Drill2} \cap \text{Drill3} = \varnothing, \ \text{Drill1} \cap \text{Drill2} = \varnothing \tag{4}$$

In this case, it is necessary to pinch stratum, relying entirely on the order of formation of the geological age as the rule to connect. Generally, the principle of judging the direction of stratum pinching is that the new stratum pinching upward and the old stratum downward. However, in the real geological situation, there is also a special case of stratigraphic inversion. Any strata with an inverted stratigraphic sequence are connected by pinching with the old strata on top and the new strata on the bottom.

In the previous classification results, there are eight cases with entirely different compositions of GTP drills. Figure 15 illustrates specific combinations, representing the occurrence of stratigraphic pinch-out in real geological tectonic events (Fig. 15 - center).

(3) Combination of correlation-based and stratigraphic chronological order-based linkage

The combination of correlation-based linkage and stratigraphic chronological order-based linkage refers to the
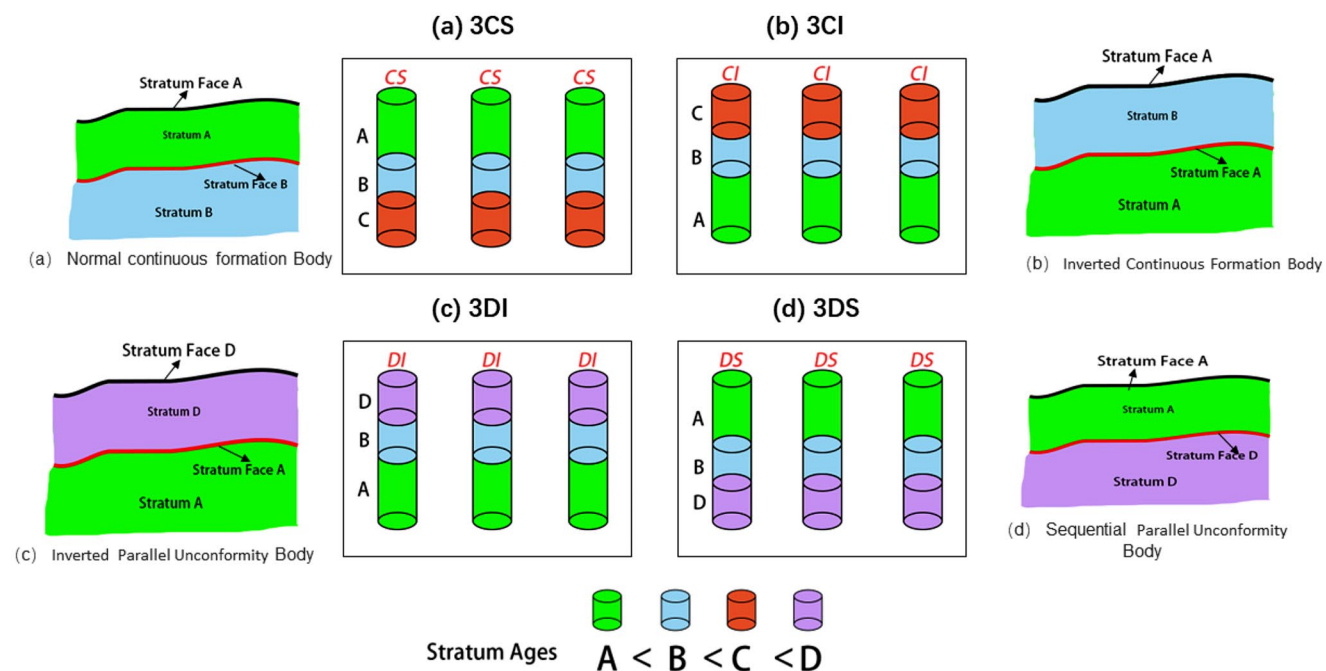

Fig. 13 Four identical drilling combinations. (**a**) Normal continuous fomation Body. (**b**) Inverted Continuous Foemation Body. (**c**) Inverted Parallel Unconformity Body. (**d**) Seguenfial Parallel Unconformity Body
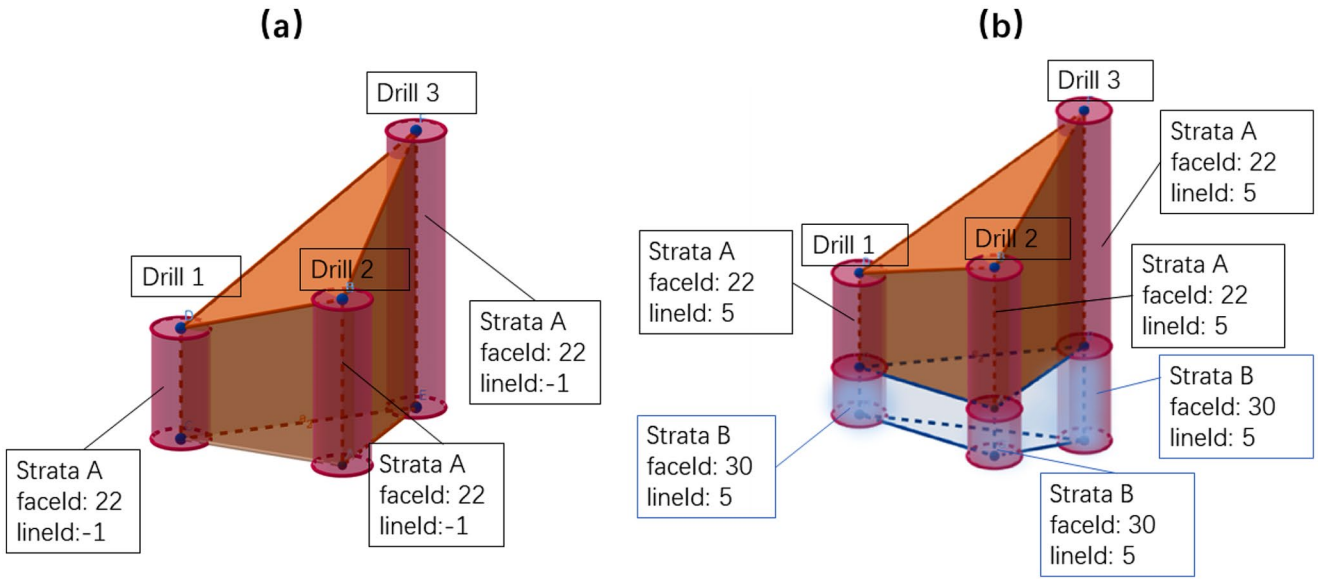
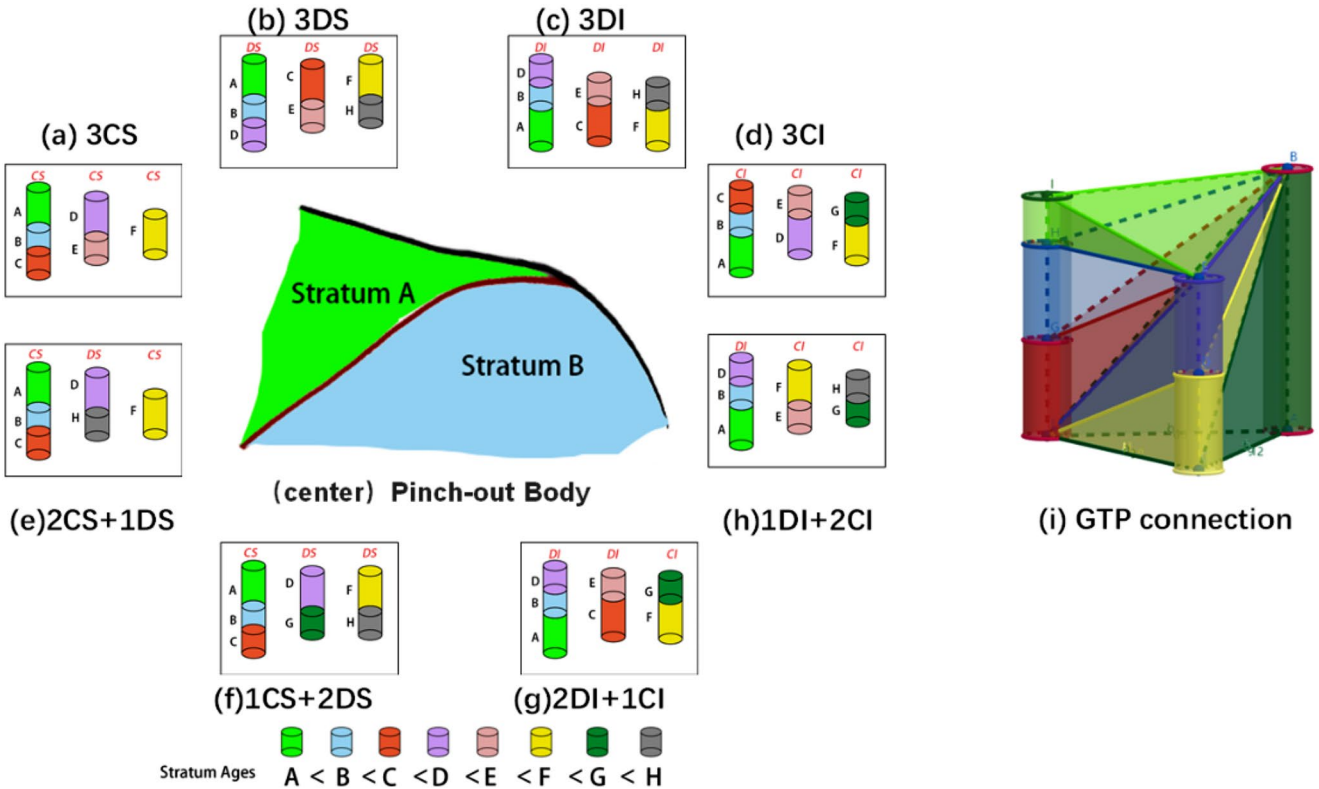**Fig. 14** Virtual stratification is exactly the same. (**a**) Single layer GTP. (**b**) Multi-layer GTP

Fig. 15 GTP connection rules using only the sequence of new and old formations. (**a**) 3CS. (**b**) 3DS. (**c**) 3DI. (**d**) 3CI. (**e**) 2CS+1DS. (**f**) 1CS+2DS. (**g**) 2DI+1CI. (**h**) 1DI+2CI. (center) Pinch-out Body

simultaneous use of both of these rules to connect virtual drills. Figure 16 illustrates the drill combinations that adhere to the composite rule and their corresponding GTP linkage results. In cases where the virtual drills display sequential stratigraphy, both sequential geo-rules (new stratigraphy on top, old stratigraphy on the bottom) and correlation information are employed, as depicted in Fig. 16(a, b, e, f). For inverted strata, the geologic age rule of correlation + inversion is necessary, as shown in Fig. 16(c, d, g, h).
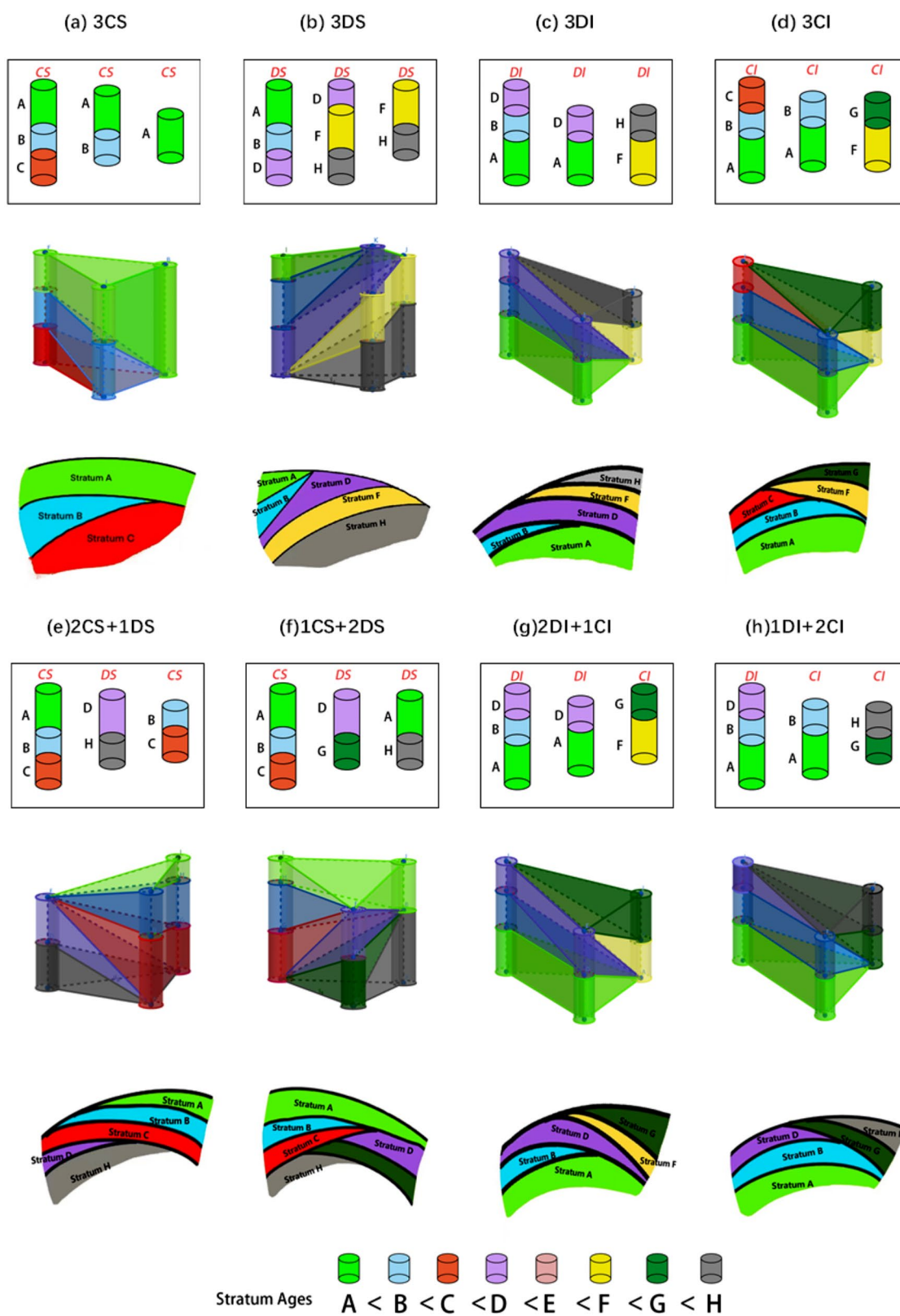
Fig. 16 Examples of drilling combinations that require the use of two connection rules simultaneously. (**a**) 3CS. (**b**) 3DS. (**c**) 3DI. (**d**) 3CI. (**e**) 2CS+1DS. (**f**) 1CS+2DS. (**g**) 2DI+1CI. (**h**) 1DI+2CI

Experimentation and analysis

Due to the complex stratigraphy and surface undulation in the real experimental area, visualizing the method's modeling results on typical tectonic phenomena in geology is challenging. To address this, the paper initially presents four classical simulation experimental areas. Subsequently, a rare complex inverted fold simulation experiment, seldom encountered in real geological environments, showcases the method's modeling effect on special geological structures. Finally, a research-significant real experimental area is selected, and the results are verified by comparing them with hand-drawn profiles from expert data.

Simulation experiments

Overview of the experimental area

This paper focuses on four selected classic layered geological formations: anticline, syncline, monocline and inverted monocline formation. Figure 17 illustrates the tectonic process and 2D geological map of these formations.

(1) Simulation experiment 1: anticline folds

The axial plane of the anticline fold in simulation experiment 1 is upright. The two limbs are symmetrically distributed and the dip angle is 45 degrees. Figure 17a, b show the process from ordinary sedimentary strata to the formation of the backslope and its outcrop. Figure 17c shows its 2D geological map. In order to simplify the calculation, the

Fig. 17 Overview of simulation experiment areas. (**a**) ~(**b**) Formation of Anticline. (**c**) 2D Geological Map of Anticline. (**d**) ~(**e**) Formation of Syncline. (**f**) 2D Geological Map of Syncline. (**g**) ~(**h**) Formation of Monocline. (**i**) 2D Geological Map of Monocline. (**j**) ~(**k**) Formation of inverted Monocline. (**l**) 2D Geological Map of Inverted Monocline
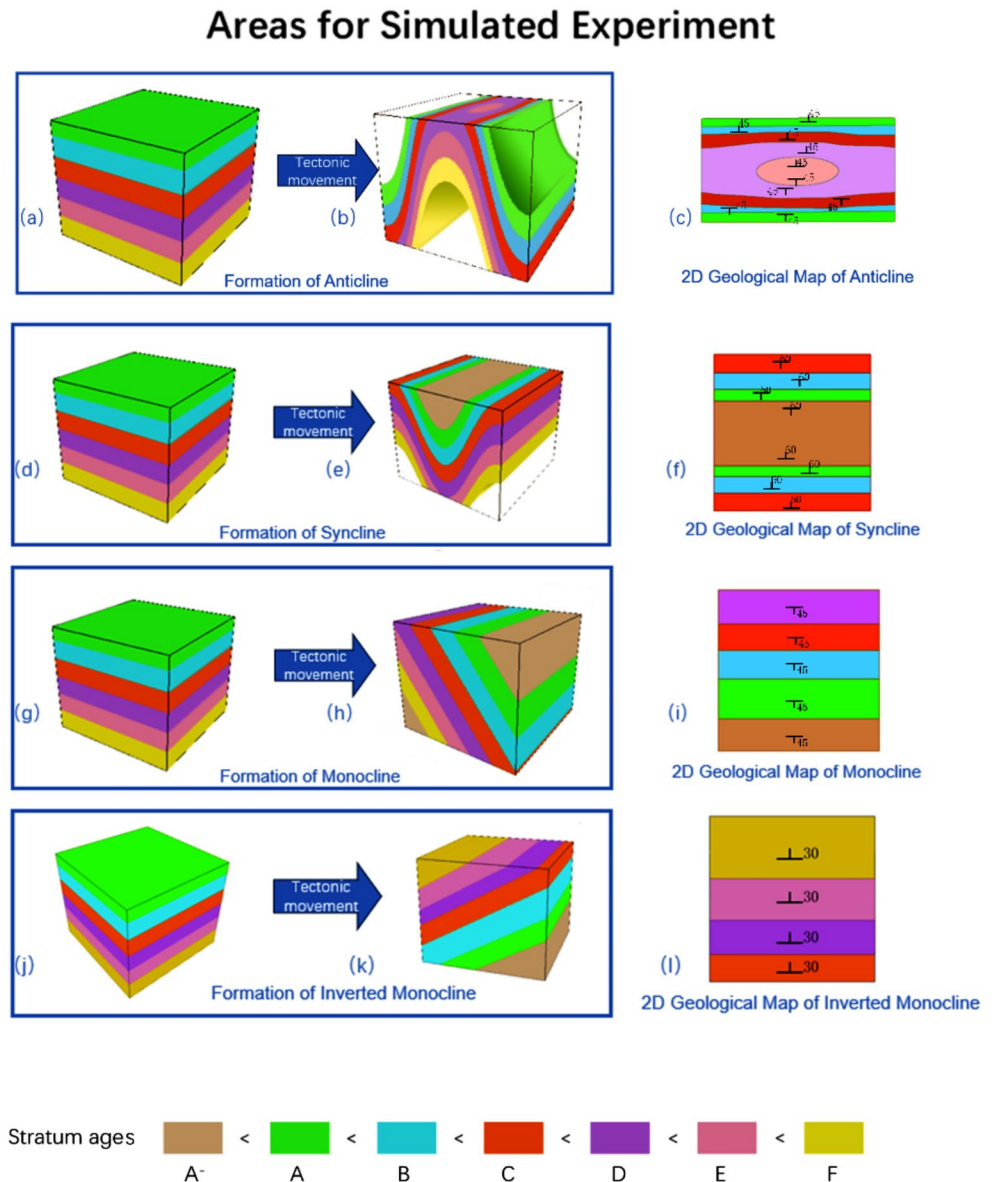
bedrock elevation surface of the simulated experimental area is set as a uniform elevation.

(2) Simulation experiment 2: syncline folds

The syncline folds in simulation experiment 2 are also upright in the axial plane, symmetrically distributed on both limbs and with a dip angle of 60 degrees. Figure 17d, e shows its tectonic process, and Fig. 17f shows its 2D geological map.

(3) Simulation experiment 3: monocline tectonics

The monocline tectonic strike in simulated experiment 3 is to the north, the dip is to the east, and the dip angle is 45 degrees. Figure 17g~17, h show its tectonic process. Figure 17i shows its 2D geological map.

(4) Simulation experiment 4: inverted monocline tectonics

The inverted monocline tectonic structure in simulation experiment 4 is oriented to the north and dips to the west with an inclination of 30 degrees. Figure 17i-l show the tectonic process. Figure 17l shows the 2D geological map, and the legend shows the age sequence and color scheme of the simulated strata.

(5) Simulation experiment 5: complex inverted folds

The axis of the inverted fold tends to be oriented in the southeast direction (Fig. 18b), with dip angles varying from 10 to 75°. Additionally, there are strike-slip faults. Figure 18c-e illustrate the geotectonic processes of the inverted folds. Figure 18c shows the original folds and their inclined surfaces. Figure 18d depicts the weathering or stripping surfaces. Figure 18d displays the rock outcrop after weathering or stripping. Figure 18e presents a schematic diagram of the rock mass after horizontal sliding fracture movement. It corresponds to the 2D geological map of Fig. 18a, where stratum E is not an inverted fold but rather another sedimentary layer. The 2D geological map includes not only normal sedimentary strata but also sequential unconformities, inverted parallel unconformities, and inverted continuous sedimentary strata. Stratigraphic pinch-out occurs at certain junctions.

Modeling results and analysis

The 2D geological maps of the simulated areas underwent information mining and GTP body element model construction. Results are shown in Fig. 19. Figure 19a4 illustrate the anticline fold modeling outcomes, including map-cut sections (19a1), virtual drills on a section (19a2), and virtual drill points on the planar surface (19a3). A segmentation operation revealed the internal structure of the anticline fold. Cross-sectional model results are displayed in Fig. 19a5. It is obvious from the cross-sectional results that the axial surface of this anticline fold is upright. The two
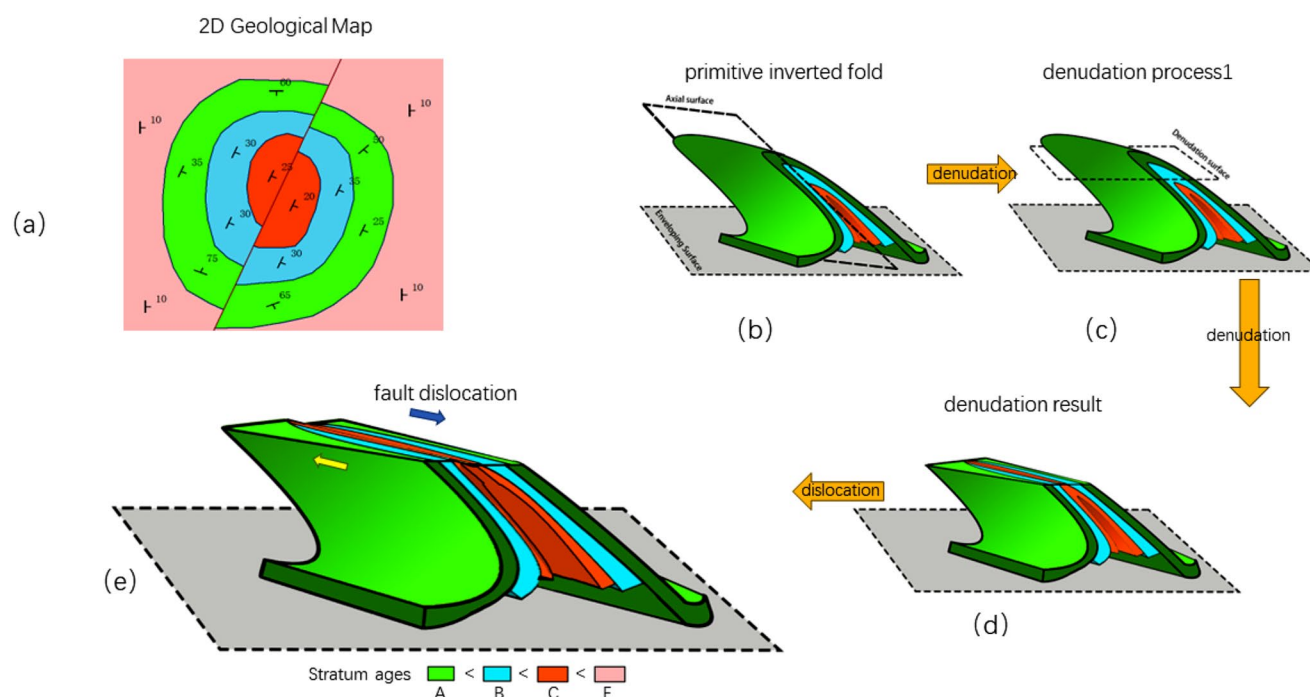

Fig. 18 2D Geological Map of Inverted Fold for Simulated Experiment. (**a**) 2D Geological Map. (**b**) primitive inverted fold. (**c**) denudation process1. (**d**) denudation result. (**e**) Toward a sliding inverted fold final result
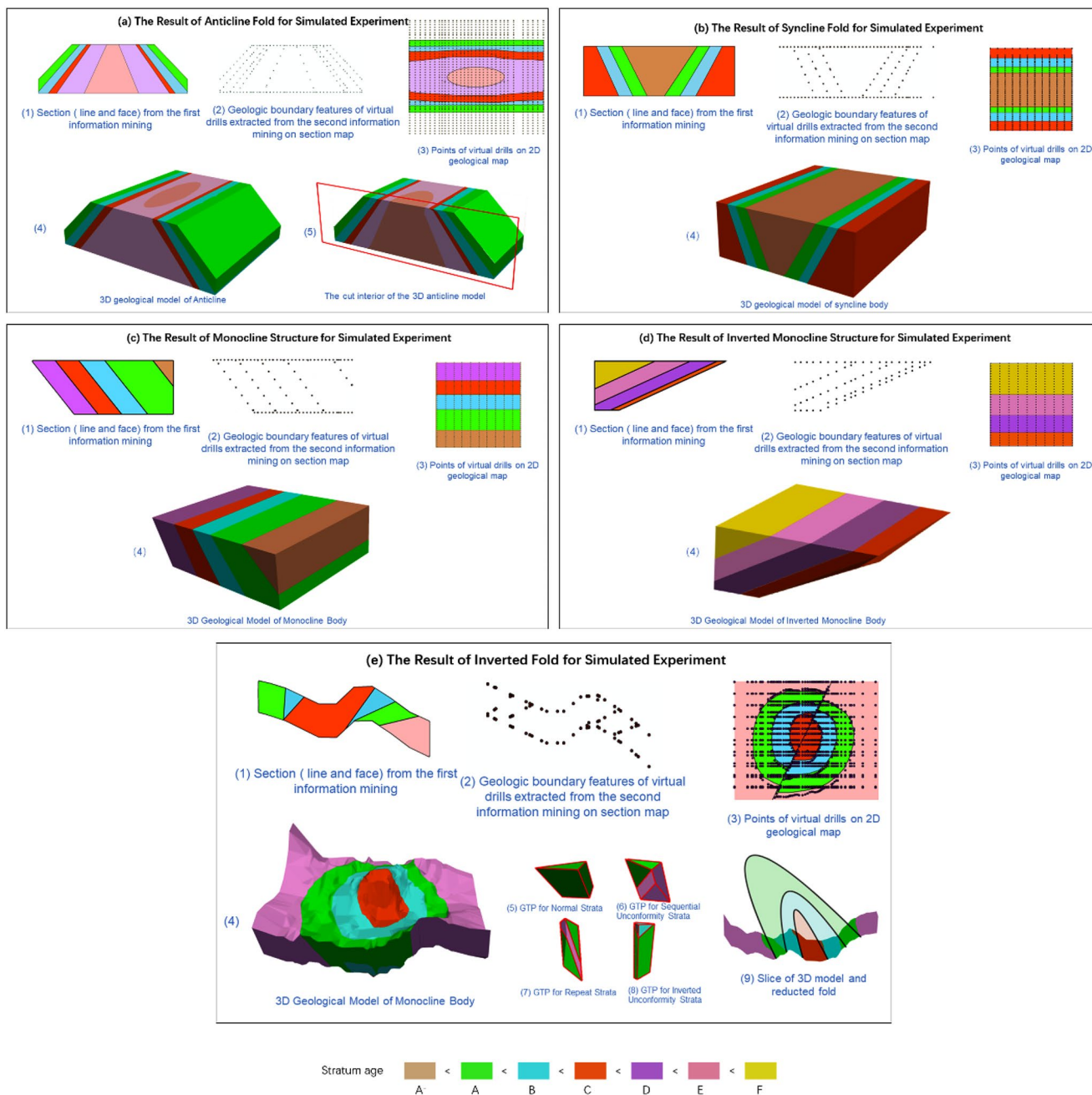
Fig. 19 Results of Simulated Experiments. (**a**) The Result of Anticline Fold for Simulated Experiment. (**b**) The Result of Syncline Fold for Simulated Experiment. (**c**) The Result of Monocline Structure for Simulated Experiment. (**d**) The Result of Inverted Monocline Structure for Simulated Experiment. (**e**) The Result of Inverted Fold for Simulated

Experiment. The next level of headings for each sub-module are as follows: (1) Section (line and face) from the first information mining; (2) Geologic boundary features of virtual drills extracted from the second information mining on section map; (3) Points of virtual drills on 2D geological map; (4) 3D geological model of Anticline

flanks are symmetrically distributed, and the dip angle is 45 degrees. It is consistent with our expected results. Similarly, Fig. 19b4 show the modeling outcomes of the anticline fold, and Fig. 19c-d present the monocline structure results, providing insights into tectonic morphology and spatial arrangement of the strata. The anticline folds are also axially oriented, with symmetrical distribution of the two

limbs and an inclination of about 60 degrees. The modeling results of the monocline formations also show that their occurrences are in perfect agreement with the original data. These four simulation experiments can show that our algorithm is excellent in modeling classical bedrock geological formations. Figure 19d4 shows the modeling results of the inverted monocline structure. Due to its small angle of dip,

it leads to the situation of multi-layer stacked inverted strata. This simulation experiment can illustrate the effectiveness of our algorithm in dealing with multilayered inverted geological bodies.

Figure 19e4 displays the modeling results for the inverted fold simulation area. The GTP body element model in Fig. 19e5 represents normal depositional stratigraphy for a correlation-based connectivity rule. Figure 19e6 represents sequentially unconformable strata, while Fig. 19e7 depict stratigraphic duplications. The GTP with three virtual drills in Fig. 19e8 represents an inverted unconformity stratigraphy, using the inverted geologic age rule and correlation information for connectivity. Pinch-out occurs in all Fig. 19e6-8. Figure 19e9 is a section derived from the 3D model. Combining its fold morphology with simulated stratigraphic order, the structure is identified as an inverted fold with aligned axial dip and dip angle as described in the simulated data.

Through the above four simulation experiments, we have not only proved that the modeling method proposed in this paper is excellent on classical geological formations, but also proved the correctness of the modeling effect of the method on very special and complex geological formations.

Real experiments

Overview of the experimental area

According to geological research data, the Mufu Mountain complex anticline (Fig. 20) in Nanjing, Jiangsu Province, China, spans approximately 4 km from north to south and 6 km from east to west. The complex anticline belongs to the Ningzhen Mountain Range, which consists of the
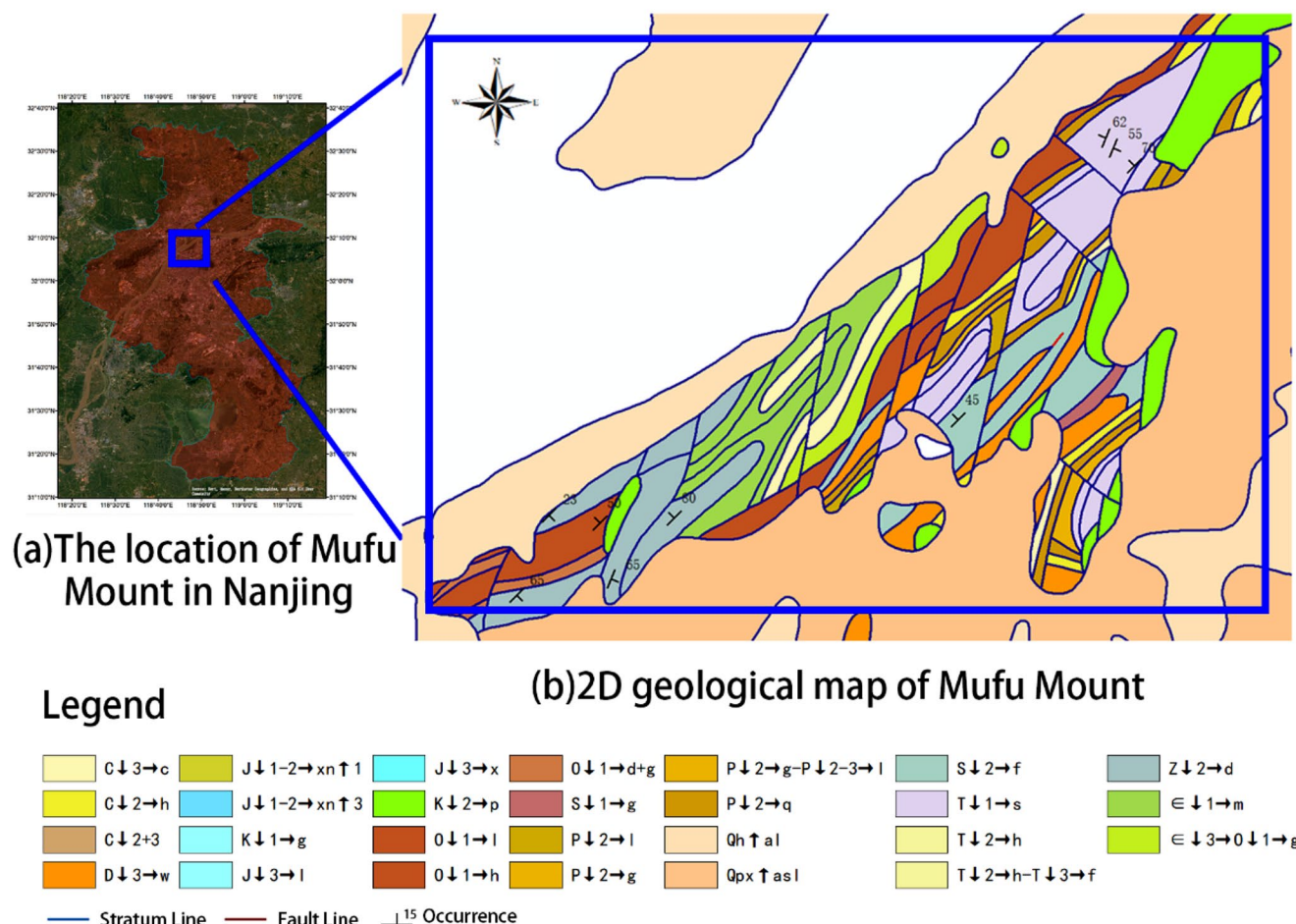

Fig. 20 Topographic and geologic Map of Study Areas in Nanjing. (a) The location of MufMount in Nanjing. (b) 2D geological map of Mufu Mount

Aurignacian-Triassic system, with the core composed of the Aurignacian and Cambrian. The axial direction of the anticline is 45–60°. The northwest wing is damaged by faults, forming a steep fault cliff along the river, with a strata dip angle reaching about 70–80°. The southeast wing is relatively intact, consisting of Paleozoic and Lower Triassic formations. The rock strata close to the core are slightly tilted towards the southeast, and the dip angle of the wing decreases. The southeast wing of the complex backslope exhibits tighter secondary folds with four secondary dorsal slopes and five secondary dipping slopes. The axes of these folds tilt to the northwest with a dip angle of about 80°. The axes of the backslope also tilt to the northwest with a dip angle of about 80°. There are mainly four secondary dorsal slopes and five secondary obliquities, with the axes inclined to the northwest at an angle of about 80°, and the dorsal slope axes dipping to the northeast.

The associated backlash faults with the secondary folds are extensively developed, with more than 20 northeast-trending backlash faults within a width of less than 2 km along the direction of the main folds. Almost all stratigraphic units are in fault contact with each other. The retrograde faults are characterized by a large number of faults (average 1/100 m), stable production (striking northeast, inclined to northwest, dipping angle of 70–85°), and obvious retrograde strike. These features have high research value. The region exhibits numerous faults, complex folds, and a large extent, making it suitable for three-dimensional modeling using this method. Figure 20a shows the location of the Mufu Mountain area in Nanjing, and Fig. 20b presents the 2D geological map used in this experiment, with a scale of 1:50,000.

Modeling results and analysis

In the actual experiment, the 2D geological map of the Mufu Mountain area was initially analyzed to extract information. This resulted in the generation of 161 map-cut cross sections, as shown in Fig. 21a. An example of the sequence diagram for the map-cut cross sections is displayed in the upper figure of Fig. 21b. Using these cross sections, a second information extraction was conducted to create a column of 52,606 virtual drills. The lower panel of Fig. 21b illustrates the outcome of mining a single map-cut cross
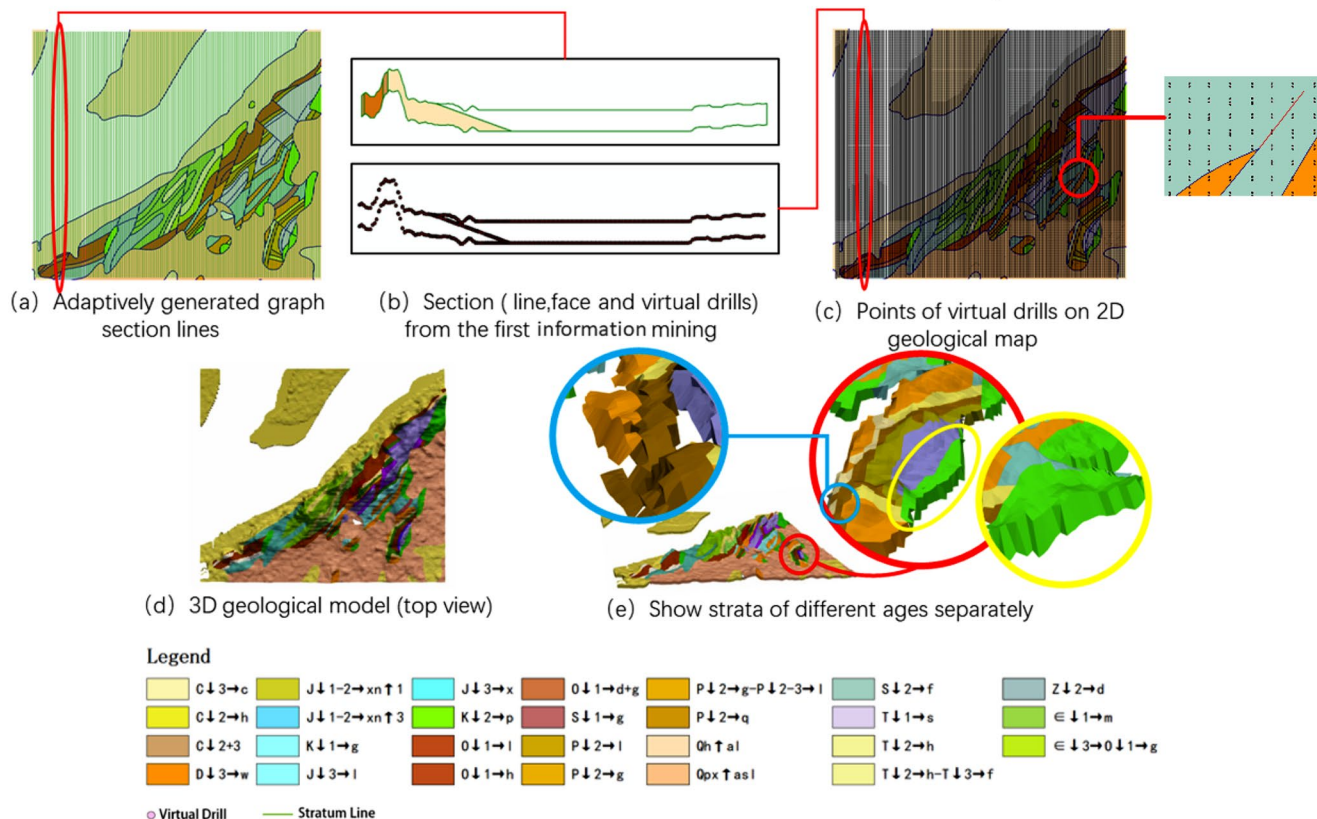

Fig. 21 3D Model of Geologic Bodies for Mufu Mount Area. (**a**) Adaptively generated graph section lines. (**b**) Section (line,face and virtual drills) from the first information mining. (**c**) Points of virtual drills on 2D geological map. (**d**) 3D geological model (top view). (**e**) Show strata of different ages separately

section to generate virtual drills on the section. The point layout of these virtual drills on the 2D geological map is depicted in Fig. 21c. Subsequently, a triangular network was constructed based on the planar point locations of these virtual drills, resulting in a total of 104,510 GTP triangular surfaces. Finally, following the GTP connection rules discussed in Sect. 3.4.2, the GTP 3D bedrock model was constructed. The top view of the modeling result is presented in Fig. 21d, while Fig. 21e showcases the side view of the model along with the stratigraphic model of different ages in blocks.

The 3D modeling results presented in this paper can be validated by creating sliced sections on the constructed 3D bedrock model. These sliced sections should be generated in the same direction and angle as the expert hand-drawn profiles from existing geological data. By comparing the sliced sections with the expert hand-drawn sections, the accuracy of the information mining and modeling results in this paper can be verified.

Comparison results were conducted between the modeled sliced section and the expert hand-drawn section at the same location in the Mufu Mountain experimental area

(22b). Figure 22a illustrates the plan view and location of the section line in the Mufu Mountain experimental area. Figure 22b shows the side view of the 3D model of the area. Figure 22c displays the top view of the constructed 3D geologic body model for the experimental area. Figure 22d demonstrates the section pulled from the constructed 3D solid model in the same direction. Figure 22e shows the restored stratigraphic folds and stratigraphic depositional conditions based on the occurrence of the stratigraphic line and the symmetry of the old and new stratigraphic layers on the section. Figure 22f presents the profile information hand-drawn by the expert over the main peak of Mufu Mountain, Lao Mountain.

From Fig. 22a, the three-dimensional model of Mufushan reveals that its north and west flanks exhibit steep fault cliffs along the Yangtze River, characterized by stratigraphic dip angles of 70–80°. The main peak of Mufushan, Laoshan, is prominently defined by syncline folds, while reverse faults are extensively developed and exhibit stability. These faults strike to the northeast and dip to the northwest, with dip angles ranging between 70–80°.

Fig. 22 Comparison and verification of the section of the 3D geological body model in Mufu Mount area with the expert hand-drawn sections. (**a**) 2D Geological Map (**b**) 3D Model Side View. (**c**) 3D Model. (**d**) Cross Section. (**e**) Reduced Cross section (**f**) Expert Hand-drawn Sections
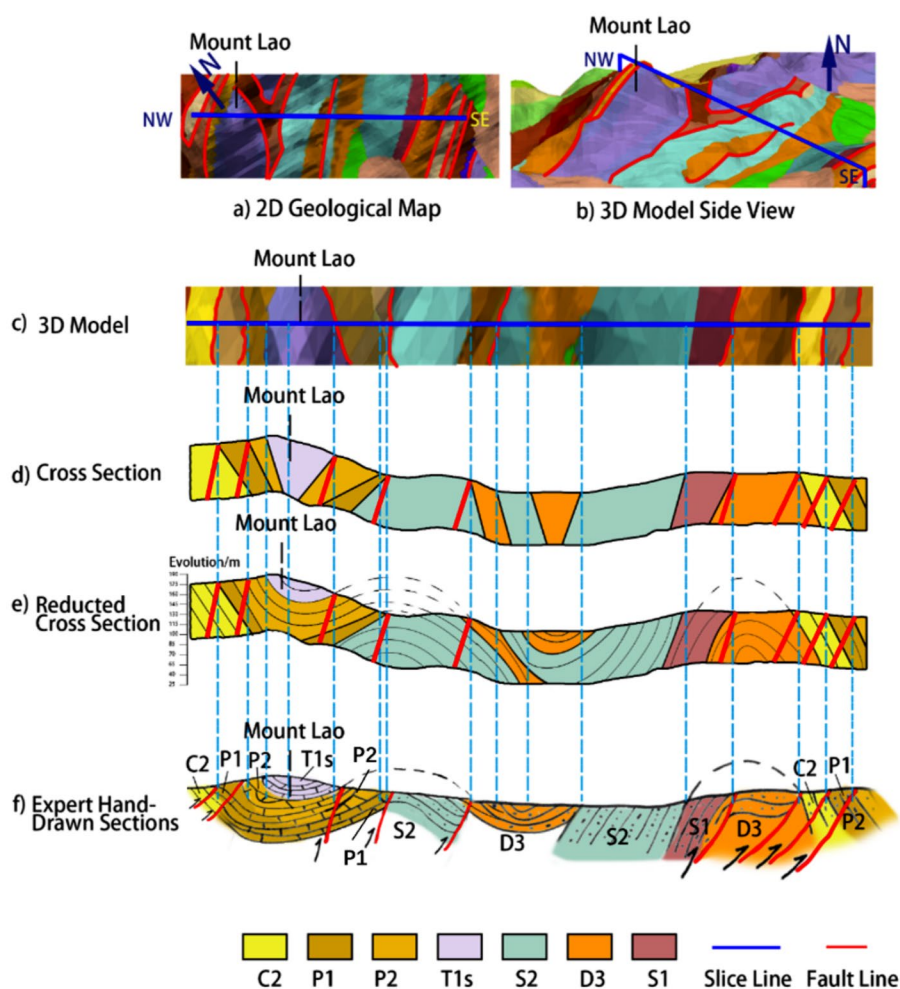
In Fig. 22b, there are slight differences observed in the profile results obtained by the model section over the main peak of Mufushan, Mt. Laoshan, compared to the expert's profile. Notably, stratum S2 appears in stratum D3 in the model section. This discrepancy can be attributed to a couple of factors. Firstly, the section length of approximately 1500 m may have influenced the representation of certain strata. Secondly, the expert utilized the wireline method to measure the geological section in the field, which allowed for the bypassing of certain strata based on field conditions. On the other hand, the modeled slice profile created in this paper does not precisely replicate the exact route of the expert's measurement; rather, it represents a straight-line profile. It is because the route used by the expert to obtain the profile may consist of a dozen or more curved, folded segments. These process documentation data are older or have not survived in the archives at all, and we have no way of examining them. It can also be seen from the 2D geological maps that there does not exist any stratigraphic arrangement through which a straight line passes that would yield expert hand-drawn results. This confirms our conjecture about the methodology used by the experts in the field to measure the geological profiles. Therefore, we are left with the most ideal method: drawing straight lines to obtain the model's profile. Hence, a slight discrepancy exists when compared to the expert's profile. However, with the exception of this specific area, the stratigraphic age and production align closely with the expert's hand-drawn profile.

Through careful comparison with the expert hand-drawn map, it is evident that the modeling method employed in this paper exhibits similarities in terms of surface undulation, rock strata layering, folding expression, and fault contact. The validation analysis conducted demonstrates that this method successfully captures the stratigraphic features of the 2D geological map in planar view and accurately represents the interstratigraphic relationships in section view. Additionally, the proposed GTP connection rules and connection results align with the stratigraphic connections as perceived by individuals. This further highlights the effectiveness and reliability of the method in preserving the essential characteristics of the geologic features and ensuring consistency with human cognition in stratigraphic interpretation.

Discussion

To demonstrate the advantages and scientific validity of the present method in terms of stratigraphic order and expression of geological formations, a comparison was made with the method used in the previous work by Lin et al. (2017) (Fig. 23). The 2D geological map underwent initial information mining to generate two adjacent map-cut sections (Fig. 23a). These two cross sections showed no correspondence between the wireframe and stratigraphic attributes. In contrast, the modeling results obtained using the present method accurately reproduced the surface outcrop formation characteristics of the original 2D geological map (Fig. 23c). However, Lin's method exhibited errors when wireframe correspondence was lacking between neighboring cross sections, as it failed to fully extract information from the 2D geological map.

To illustrate the advantage of the complex connection rule proposed by this method in Sect. 3.4.2, a separate modeling experiment was conducted, using only the new and old order of strata as the connection rule for comparison (Fig. 24). By overlaying the modeling results from both connection methods with the 2D geological map, a top view comparison was made to assess the restoration of 2D geological map features. The composite connection rule in this method closely aligned with the stratigraphic line, better reflecting the characteristics of the 2D geological map. A schematic diagram (Fig. 25) showcased the difference in GTP connections between the experimental results of the two connection methods. The GTP connection in this method (Fig. 25e) aligned more closely with the geological features on the planar geological map, while the comparison experiment (Fig. 25g) erroneously added a layer of overlying strata, resulting in modeling errors.
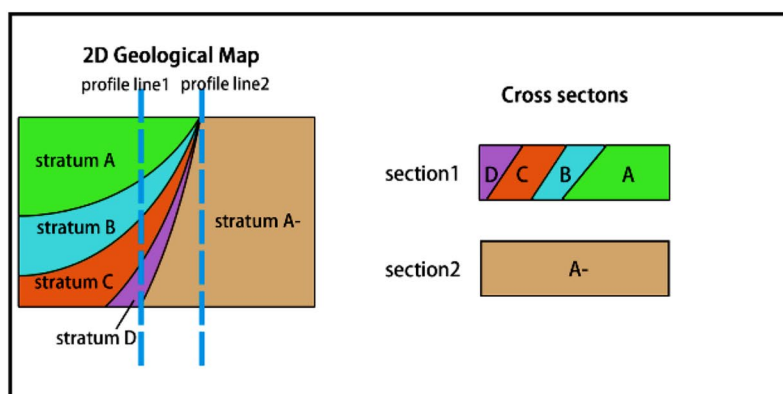
However, the present method also has limitations:

(1) It is only applicable to modeling stratified rock bodies exposed at the surface and cannot be used for non-stratified stratified rocks or unexposed rock bodies such as lenticular bodies. The proposed method also cannot be used to build the models including intrusion/extrusive rock with multi-Z-value. Moreover, mining information from inverted folds with multi-Z-value and modeling them directly from 2D geological maps can be challenging, especially in the absence of outcrops. Addressing such a situation effectively requires the aggregation of multiple data sources, including real profiles that depict the geology of various subsurface layers. This approach provides valuable insights for our ongoing work and paves the way for further research on related issues. Furthermore, our future research will persist in exploring 3D geological modeling for real geological profiles.
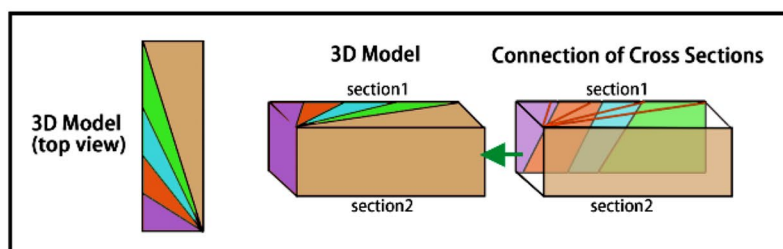
(2) The accuracy of the model is greatly influenced by the scale of the 2D geological map, with finer geological information obtained at larger scales.

(3) The constructed model can only extend to a certain depth below the surface. To deduce the bedrock tectonic situation at greater depths, real geological drill data or physical exploration data should be introduced as additional support.
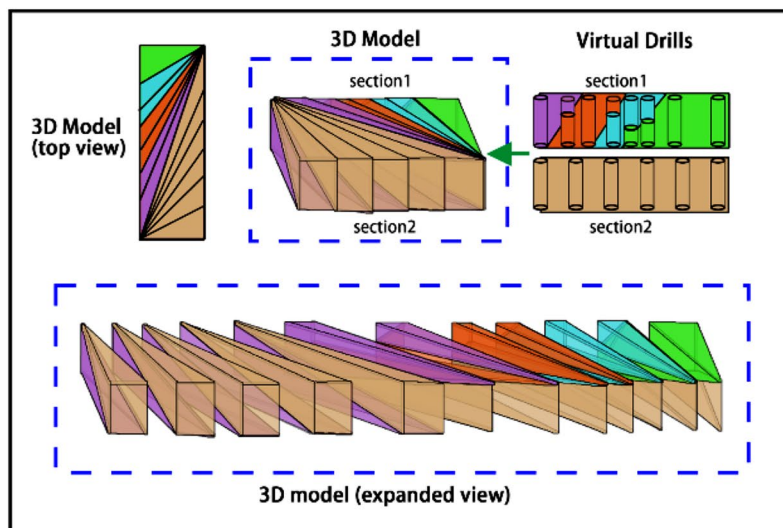
Fig. 23 Schematic diagram of connecting geological bodies according to the profile line relationship between cross sections in Lin et al. (2017) (**a**) 2D Geological Map and Cross Sections. (**b**) Modeling Process and Results Using Contour Algorithm. (**c**) Modeling Process and Results Using the Method in this Paper

(4) Although our proposed method of adaptively generating profiles along the location of stratigraphic boundary line folds and subsequently creating virtual drills yields great modeling results, the extraction of virtual drills remains dependent on the profile. Our future optimization efforts will focus on deploying virtual drills in non-profile areas.
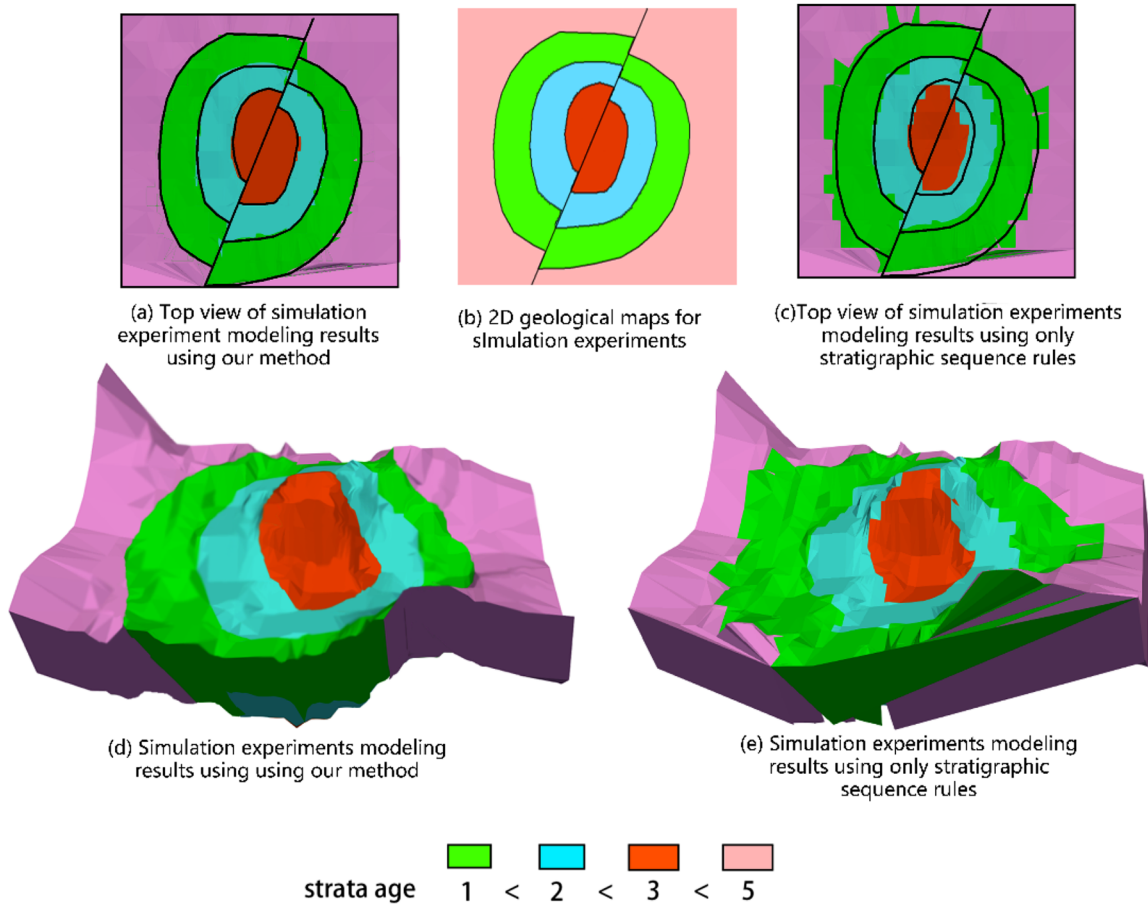
Fig. 24 Schematic Diagram of Modeling Results Comparing 2 GTP Connection Methods. (**a**) Top view of simulation experiment modeling results using our method. (**b**) 2D geological maps for sImulation experiments. (**c**) Top view of simulation experiments modeling results using only stratigraphic sequence rules. (**d**) Simulation experiments modeling results using using our method. (**e**) Simulation experiments modeling results using only stratigraphic sequence rules

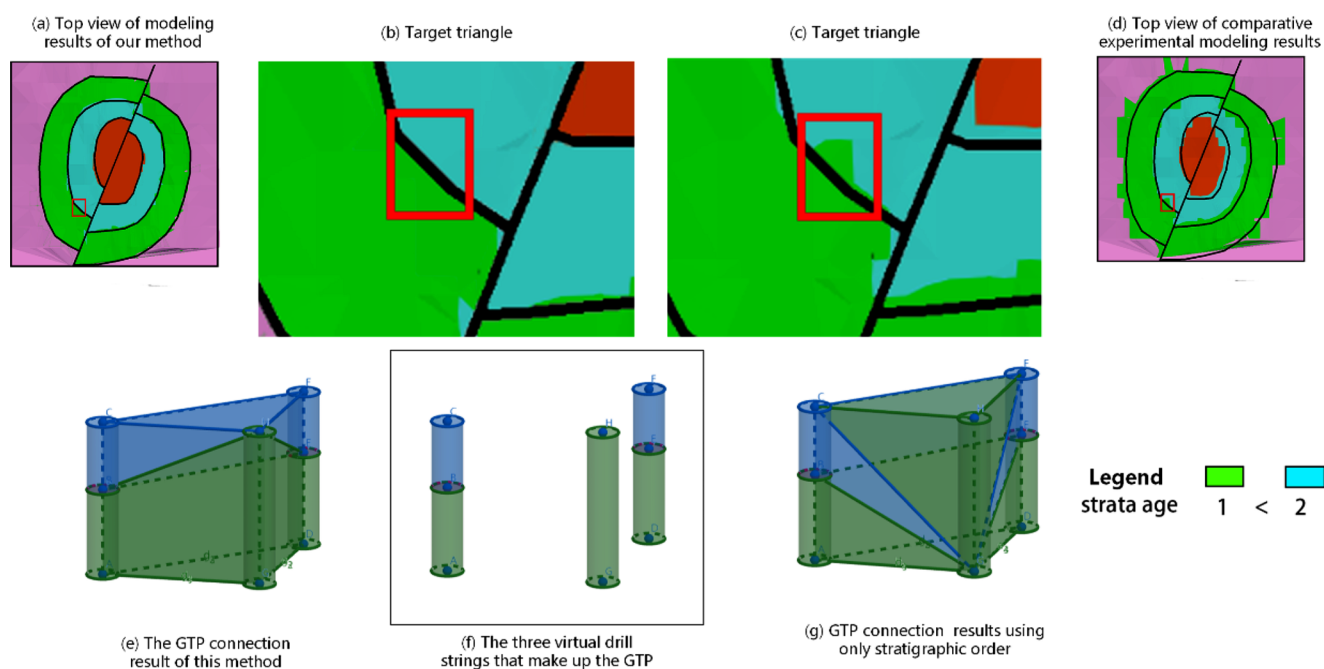## Comparison Examples of GTP Connections Results by 2 GTP Connection Methods

(a) Top view of modeling results of our method

(b) Target triangle

(c) Target triangle

(d) Top view of comparative experimental modeling results

(e) The GTP connection result of this method

(f) The three virtual drill strings that make up the GTP

(g) GTP connection results using only stratigraphic order

Legend
strata age 1 < 2

Fig. 25 Schematic diagram of the processing results of two connection rules for inverted strata. (**a**) Top view of modeling results of our method. (**b**) Target triangle. (**c**) Target triangle. (**d**) Top view of comparative experimental modeling results. (**e**) The GTP connection result of this method. (**f**) The three virtual drill strings that make up the GTP. (**g**) GTP connection results using only stratigraphic order

Conclusion

In this paper, a method is proposed to address challenges encountered when modeling 3D bedrock models, such as limited availability of large-scale data and the complexity of modeling intricate geological formations. The proposed method focuses on extracting geological information from 2D geological maps to facilitate three-dimensional bedrock modeling. The method adopts an adaptive approach to generate sequential map-cut sections, enabling the extraction of geological information from the 2D geological map. This includes features like surface undulation, occurrence, topological relationships, stratigraphy, stratigraphic age, and more. Additionally, the method incorporates a virtual drill data structure to extract information from the map-cut sections. Throughout both stages of information extraction, the mapping relationship between the 2D geological map, map-cut section, and virtual drill is consistently maintained as associated information.

Meanwhile, this paper introduces the GTP as a spatial data model for integrating discrete information from virtual drills into the modeling process. The combination of real geological phenomena, virtual drills, and GTP is categorized from two classification perspectives: descriptive and identical. Additionally, three specific rules are proposed to

address GTP stratigraphic connections. Finally, the paper generates a 3D bedrock model.

The results of the example modeling demonstrate that the proposed method effectively utilizes 2D geological maps in the absence of data such as measured drills and sections. This enables the extraction of extensive geological information and the construction of a high-quality, large-scale three-dimensional bedrock model. The method also preserves the geological features present on the planar surface and accurately simulates the characteristics of the geological body.

Furthermore, the constructed model provides a more accurate representation of geological phenomena such as stratigraphic stratigraphic pinch-out, and inter-stratigraphic contact relationships. The introduction of the GTP body element model further facilitates the evaluation and utilization of urban underground resources in the future. Additionally, it supports the demand for automated construction of large-scale 3D bedrock models. Our future research will persist in exploring 3D geological modeling for real geological profiles.

Author contributions Tong Niu: Conceptualization, Data curation, Formal analysis, Investigation, MethodologySoftware, Visualization, Writing – original draft, Writing – review & editingBingxian Lin: Corresponding author, Conceptualization, Funding acquisition, Supervision, Validation, Writing – review & editingLiangchen Zhou:

Declarations

Competing interests The authors declare no competing interests.

References

Abbaszadeh Shahri A, Larsson S, Renkel C (2020) Artificial intelligence models to generate visualized bedrock level: a case study in Sweden. Model Earth Syst Environ 6:1509–1528

Cai B, Zhao J, Yu X (2019) A methodology for 3D geological mapping and implementation. Multimedia Tools Appl 78:28703–28713

Che D, Jia Q (2019) Three-Dimensional Geological modeling of coal seams using Weighted Kriging Method and Multi-source Data. IEEE Access 7:118037–118045

Chen Y, Li A, Lv G, Xie X (2023) An automated method for topology consistent processing of parallel geological cross-sections based on topology reasoning. Comput Geosci 180:105442

Compton RR, Compton RR (1985) Geology in the field. Wiley, New York

Dhont D, Luxey P, Chorowicz J (2005) 3-D modeling of geologic maps from surface data. AAPG Bull 89:1465–1474

Frank T, Tertois A, Mallet J (2007) 3D-reconstruction of complex geological interfaces from irregularly distributed and noisy point data. Comput Geosci 33:932–943

García-Gil A, Baquedano C, Marazuela MÁ, Martínez-León J, Cruz-Pérez N, Hernández-Gutiérrez LE, Santamarta JC (2023) A 3D geological model of El Hierro volcanic island reflecting intraplate volcanism cycles. Groundw Sustainable Dev 21:100936

Gong W (2019) Virtual display system of geological body based on key algorithms of three-dimensional modelling. J Comput Methods Sci Eng 19:107–113

Guo J, Wang X, Wang J, Dai X, Wu L, Li C, Li F, Liu S, Jessell MW (2021) Three-dimensional geological modeling and spatial analysis from geotechnical borehole data using an implicit surface and marching tetrahedra algorithm. Eng Geol 284:106047

Hao T, Xu Y, Li Z, Xing J (2016) Integration of geophysical constraints for multilayer geometry refinements in 2.5D gravity inversion. Geophysics Journal of the Society of Exploration Geophysicists

Hao M, Li M, Zhang J, Liu Y, Huang C, Zhou F (2021) Research on 3D geological modeling method based on multiple constraints. Earth Sci Inf 14:291–297

He W, Wu W (2013) Study on Algorithm for Grid subdivision and encryption based on technology of three Dimensional Geological modeling. Appl Mech Mater 336–338:1416–1421

Herbert M, Jones C, Tudhope D (1995) Three-dimensional reconstruction of geoscientific objects from serial sections. Visual Comput 11:343–359

Hou W, Wu X, Liu X, Chen G (2007) A complex fault modeling method based on geological plane map. 28:169–172

Høyer AS, Jørgensen F, Foged N, He X, Christiansen AV (2015) Three-dimensional geological modelling of AEM resistivity data — a comparison of three methods. J Appl Geophys 115:65–78

Jessell M (2001) Three-dimensional geological modelling of potential-field data. Comput Geosci 27:455–465

Jørgensen F, Møller R, Nebel L, Jensen N, Christiansen A, Sandersen P (2013) A method for cognitive 3D geological voxel modelling of AEM data. Bull Eng Geol Environ 72:421–432

Kaufmann O, Martin T (2008) 3D geological modelling from boreholes, cross-sections and geological maps, application over former natural gas storages in coal mines. Comput Geosci 34:278–290

Li C, Wu Z, Yang Y, Hua C (2019) Modeling method and case study of drillhole data based on GOCAD. 37(1):125–130Jiangxi Science

Lin B, Zhou L, Lv G, Zhu A (2017) 3D geological modelling based on 2D geological map. Ann GIS 23:117–129

Liu X, Li A, Chen H, Men Y, Huang Y (2022) 3D modeling method for Dome structure using Digital Geological Map and DEM. ISPRS International Journal of Geo-Information

Ltd MG (2007) Geological Models, Rock Properties, and the 3D Inversion of Geophysical Data

Lysdahl AK, Christensen CW, Pfaffhuber AA, Vöge M, Andresen L, Skurdal GH, Panzner M (2022) Integrated bedrock model combining airborne geophysics and sparse drillings based on an artificial neural network. Eng Geol 297:106484

Malehmir A, Thunehed H, Tryggvason A (2008) The Paleoproterozoic Kristineberg mining area, northern Sweden: results from integrated 3D geophysical and geologic modeling, and implications for targeting ore deposits. Geophysics 74:B9–B22

Marrett R, Bentham PA (1997) Geometric analysis of hybrid fault-propagation/detachment folds. J Struct Geol 19:243–248

Martelet G, Calcagno P, Gumiaux C, Truffert C, Bitri A, Gapais D, Brun JP (2004) Integrated 3D geophysical and geological modelling of the Hercynian Suture Zone in the Champtoceaux area (south Brittany, France). Tectonophysics 382:117–128

Meng Y, Xu W, Tian B, Li M (2009) Method of modeling 3D geological modeling and its application based on Constraint Delaunay Triangulation. J Syst Simul 21:5985–5989

Pierantoni P, Deiana G, Galdenzi S (2013) Stratigraphic and structural features of the Sibillini Mountains (Umbria-Marche Apennines, Italy). Ital J Geosci 132:497–520

Ragan D, Mackenzie, and Ragan (1985) Structural geology. Wiley

Schetselaar EM (1995) Computerized field-data capture and GIS analysis for generation of cross sections in 3-D perspective views. Comput Geosci 21:687–701

Wu L (2004) Topological relations embodied in a generalized tri-prism (GTP) model for a 3D geoscience modeling system. Comput Geosci 30:405–418

Wu Q, Xu H, Zou X (2005) An effective method for 3D geological modeling with multi-source data integration. Comput Geosci 31:35–43

Wycisk P, Hubert T, Gossel W, Neumann C (2009) High-resolution 3D spatial modelling of complex geological structures for an environmental risk assessment of abundant mining and industrial megasites. Comput Geosci 35:165–182

Xin, He, Julian, Koch, Torben O, Sonnenborg, Flemming, Jrgensen C (2014) Transition probability-based stochastic geological modeling using airborne geophysical data and borehole data. Water Resour Res 50:3147–3169

Xu F (2014) Geological Knowledge Rule Constructing and 3D Modeling Based on Planar Geological Map. Ph.D. Thesis. Nanjing Normal University, Nanjing, China

Yang F, Wang G, Santosh M, Li R, Tang L, Cao H, Guo N, Liu C (2017) Delineation of potential exploration targets based on 3D geological modeling: a case study from the Laoangou Pb-Zn-Ag polymetallic ore deposit, China. Ore Geol Rev 89:228–252

Zanchi A, Francesca S, Stefano Z, Simone S, Graziano G (2009) 3D reconstruction of complex geological bodies: examples from the alps. Comput Geosci 35:49–69

Zhang X, Zhang J, Tian Y, Li Z, Zhang Y, Xu L, Wang S (2020) Urban geological 3D modeling based on Papery Borehole Log. ISPRS Int J Geo-Information 9:389

Zhang P, Zhang D, Yang Y, Zhang W, Wang Y, Pan Y, Liu X (2022) A Case Study on Integrated Modeling of Spatial Information of a Complex Geological Body. Lithosphere 2022

Zhou L, Lin B, Wang D, Lv G (2013) 3D geological modeling method based on Planar Geological Map. Geo-information Sci 15:32–38

Zhu L, He Z, Pan X, Wu X (2006) An Approach to Computer Modeling of Geological Faults in 3D and an application. J China Univ Min Technol 16:461–465

Zhu H, Huang X, Li X, Zhang L, Liu X (2016) Evaluation of urban underground space resources using digitalization technologies. Undergr Space 1:124–136